J Neurophysiol 119: 145–159, 2018.
First published September 27, 2017; doi:10.1152/jn.00551.2017.

RESEARCH ARTICLE | *Higher Neural Functions and Behavior*

Breathing above the brain stem: volitional control and attentional modulation in humans

Jose L. Herrero,[1,2] Simon Khuvis,[1,2] Erin Yeagle,[1,2] Moran Cerf,[3] and Ashesh D. Mehta[1,2]
[1]*The Feinstein Institute for Medical Research, Manhasset, New York;* [2]*Department of Neurosurgery, Hofstra Northwell School of Medicine, Manhasset, New York; and* [3]*Interdepartmental Neuroscience Program and Kellogg School of Management, Northwestern University, Evanston, Illinois*

Submitted 21 July 2017; accepted in final form 26 September 2017

Herrero JL, Khuvis S, Yeagle E, Cerf M, Mehta AD. Breathing above the brain stem: volitional control and attentional modulation in humans. *J Neurophysiol* 119: 145–159, 2018. First published September 27, 2017; doi:10.1152/jn.00551.2017.—Whereas the neurophysiology of respiration has traditionally focused on automatic brain stem processes, higher brain mechanisms underlying the cognitive aspects of breathing are gaining increasing interest. Therapeutic techniques have used conscious control and awareness of breathing for millennia with little understanding of the mechanisms underlying their efficacy. Using direct intracranial recordings in humans, we correlated cortical and limbic neuronal activity as measured by the intracranial electroencephalogram (iEEG) with the breathing cycle. We show this to be the direct result of neuronal activity, as demonstrated by both the specificity of the finding to the cortical gray matter and the tracking of breath by the gamma-band (40–150 Hz) envelope in these structures. We extend prior observations by showing the iEEG signal to track the breathing cycle across a widespread network of cortical and limbic structures. We further demonstrate a sensitivity of this tracking to cognitive factors by using tasks adapted from cognitive behavioral therapy and meditative practice. Specifically, volitional control and awareness of breathing engage distinct but overlapping brain circuits. During volitionally paced breathing, iEEG-breath coherence increases in a frontotemporal-insular network, and during attention to breathing, we demonstrate increased coherence in the anterior cingulate, premotor, insular, and hippocampal cortices. Our findings suggest that breathing can act as an organizing hierarchical principle for neuronal oscillations throughout the brain and detail mechanisms of how cognitive factors impact otherwise automatic neuronal processes during interoceptive attention.

NEW & NOTEWORTHY Whereas the link between breathing and brain activity has a long history of application to therapy, its neurophysiology remains unexplored. Using intracranial recordings in humans, we show neuronal activity to track the breathing cycle throughout widespread cortical/limbic sites. Volitional pacing of the breath engages frontotemporal-insular cortices, whereas attention to automatic breathing modulates the cingulate cortex. Our findings imply a fundamental role of breathing-related oscillations in driving neuronal activity and provide insight into the neuronal mechanisms of interoceptive attention.

intracranial EEG; interoceptive attention to breathing; cortical control of breathing; mind-body; oscillations

INTRODUCTION

A wealth of historical literature has focused on automatic breathing driven by brain stem structures (Butler 2007; Tenney and Ou 1977) with more recent interest in cortical involvement (Feldman et al. 2013). While motor cortex stimulation elicits diaphragmatic contraction at expected somatotopic loci (Başar et al. 2000; Bruce and Ackerson 1986; Foerster 1936; Gandevia and Rothwell 1987), the fact that the rate of breathing can be influenced by stimulation of the hippocampus, amygdala, and insula (Frysinger and Harper 1989, 1990; Harper et al. 1998; Kaada and Jasper 1952) suggests a more complex breathing circuitry above the brain stem level. Scalp EEG (Fumoto et al. 2004; Vialatte et al. 2009), transcranial magnetic stimulation (TMS; Locher et al. 2006), and neuroimaging studies (Evans et al. 1999; McKay et al. 2002), albeit with limited spatial and temporal resolution, have implicated premotor, motor, and supplementary motor cortices in the voluntary control of breathing. More direct electrophysiological measures in rodents show local field potential (LFP) oscillations in hippocampus (Nguyen Chi et al. 2016; Tsanov et al. 2014), and the barrel (Ito et al. 2014) and prefrontal cortices (Biskamp et al. 2017) to closely track the inhalation-exhalation cycle. This link between LFP oscillations and the breathing cycle can be tracked with high temporal resolution by measuring their coherence.

The human intracranial EEG (iEEG) provides information regarding neuronal activity with high (~5 mm) spatial and millisecond temporal resolution and may be recorded in the special circumstance of invasive monitoring for epilepsy surgery (Miller et al. 2012; Zhang et al. 2015). In these clinical protocols, patients with partial epilepsy, where much of the brain is relatively normal, undergo invasive electrode sampling to define pathological regions. In these circumstances, it is possible to record from relatively normal brain regions, because much of the sampled regions lie within relatively normal cortex that lie outside of the seizure onset zone (SOZ) either for the purpose of functional mapping or to rule out their participation in the network of areas participating in seizures (Borchers et al. 2011; Hamberger et al. 2014). This provides a unique window into human brain physiology, one which we can use to study cortical control of breathing. With the use of these methods, recent reports have demonstrated a correlation between the breathing cycle and iEEG oscillatory phenomena in

Address for reprint requests and other correspondence: A. D. Mehta, Northwell Health Physician Partners Neuroscience Institute, 611 Northern Boulevard, Great Neck, NY 11021 (e-mail: amehta@northwell.edu).

limbic and neocortical areas during natural breathing (Heck DH, McAfee SS, Liu Y, Babajani-Feremi A, Rezaie R, Freeman WJ, Wheless JW, Papanicolaou AC, Ruszinko M, Kozma R, unpublished observations; Heck et al. 2017; Zelano et al. 2016). However, a detailed survey of effects across multiple intracranial sites has not been conducted. To provide further description of this circuitry, we tested for iEEG synchronization to breathing throughout a wide base of sampling across limbic and cortical areas.

Whereas memory retrieval and fear discrimination appear to be sensitive to respiratory phase, and nasal breathing produces a greater deal of iEEG coherence than mouth breathing (Zelano et al. 2016), task-dependent dynamics of this coherence with respect to attention and volitional control have not been explored (see Krupnik et al. 2015 for a related psychophysical study). Such tasks are commonly used in therapeutic practices as an effort to gain interoceptive attention and control. To gain better insight into neurophysiological mechanisms engaged in these processes, we examined the areal specificity of the change in iEEG-breath coherence while subjects performed tasks aimed at controlling the pace of the respiratory rate or increasing awareness to the respiratory cycle. Given extensive brain sampling that included frontal cortex, limbic structures, and the insula, structures known for their involvement in behavioral planning and interoceptive monitoring of body states, we expected to observe increased coherence during both tasks in these structures (Chan et al. 2015; Craig 2003a; Farb et al. 2013).

Finally, whereas oscillatory activity in the iEEG likely reflects mainly neuronal contributions, it is possible that chemical/mechanical artifacts that also follow the breathing cycle may contribute to the recorded signals (Brenner and Schaul 1990; Cardoso et al. 1983; Urigüen and Garcia-Zapirain 2015). To distinguish neuronal contributions from potential artifacts, we demonstrated that these effects are selective to gray matter vs. white matter and cerebrospinal fluid (CSF) spaces, all of which may be sampled by using depth electrodes in stereoelectroencephalography (sEEG) procedures. To further rule out potential artifactual contamination and distinguish locally generated from propagated activity, we examine the iEEG-breath cycle coherence of the iEEG gamma-band envelope, a proxy of local neuronal firing (Miller et al. 2007a, 2010b).

Table 1. *Electrode sampling: anatomical region in which each electrode contact was located, following FreeSurfer automated parcellation*

Brain Area	No. of Electrodes	No. of Subjects
Amygdala	33	4
Hippocampus	30	5
Entorhinal	4	2
Parahippocampal	9	3
Insula	55	5
Lateral orbitofrontal	55	4
Medial orbitofrontal	25	4
Pars orbitalis	9	3
Olfactory bulb*	10	3
Piriform*	9	3
Pars triangularis	24	5
Pars opercularis	25	6
Frontal-rostral middle	27	5
Frontal-caudal middle	27	4
Frontal-superior	22	4
Precentral	41	6
Paracentral	10	3
Postcentral	33	6
Cingulate-anterior	14	5
Cingulate-middle	10	5
Parietal-inferior	7	3
Parietal-superior	7	3
Precuneus	9	4
Cuneus-calcarine-occipital	12	2
Lingual	12	3
Fusiform	15	5
Temporal-middle	114	5
Temporal-inferior	43	4
Temporal-superior	93	6
Supramarginal	17	4
Transverse temporal	26	4
White matter	319	5
CSF	10	5
Total	1,137	6

Shown are the locations of all electrodes ($n = 1,137$ electrodes in 6 patients) included in the analysis of natural breathing (Figs. 2–8) after FreeSurfer parcellation (Fischl et al. 2004), the number of electrodes in each area, and the number of subjects contributing to each area. Electrodes showing any sign of abnormal epileptiform discharges were excluded from the analysis. Asterisks indicate electrode locations after FreeSurfer parcellation correction; these electrodes were automatically assigned to orbitofrontal cortex and/or the pars orbitalis region by FreeSurfer parcellation in the ventral aspect of the frontal lobe. Assignment to piriform cortex or olfactory bulb was based on visual inspection of the postimplantation MRI and CT scans (see MATERIALS AND METHODS).

MATERIALS AND METHODS

Subjects and ethics statement. Eight adults (4 women) with pharmacoresistant focal epilepsy were included in this study. All subjects underwent chronic intracranial EEG (iEEG) monitoring at North Shore University Hospital to identify epileptogenic foci in the brain for later removal. Six subjects participated in initial experiments: five were implanted with stereoelectroencephalographic (sEEG) depth arrays (PMT, Chanhassen, MN) and one, with grid and strip arrays (see Fig. 1). See Table 1 for additional details on the anatomical region in which each electrode contact was located, following FreeSurfer automated parcellation (Fischl et al. 2004). A total of 1,137 electrodes from 6 patients were included in the analysis of natural breathing (see Figs. 2–8). An additional two subjects participated in the last (arousal) experiment, all implanted with sEEG depth arrays. Electrodes showing any sign of abnormal epileptiform discharges, as identified in epileptologists' clinical reports, were excluded from the analysis. All included iEEG time series were manually inspected for signal quality and were free from interictal spikes. Respiration traces were also manually inspected and excluded if unstable. All research protocols were approved and monitored by the institutional review board at the Feinstein Institute for Medical Research, and informed written consent to participate in research studies was obtained from each subject before implantation of electrodes. The decision to implant, the electrode positions, and the timing of the electrode-removal procedure were made entirely on clinical grounds, without reference to this investigation.

Whereas the proposed studies are carried out in subjects who have brain abnormalities, their physiology is generalizable to nonpathological human brains because *1*) all subjects included in this study had partial epilepsy, in which electrographic abnormalities were restricted to one portion of the brain; *2*) a large subset of the electrodes (~90%) were implanted into normal brain areas to identify functional areas and other areas to exclude from surgical resection; *3*) electrodes lying within pathological areas were excluded from all analyses; and *4*) all eight patients had Full Scale IQ scores within the average range (>90) with spared attention, short-term memory, and interoceptive abilities, according to preoperative neuropsychological testing (NIH Toolbox;

Gershon et al. 2013). The present study was carried out during the approximately 2-wk period following admission into the epilepsy monitoring unit for clinically indicated seizure-capture and mapping of sensorimotor and cognitive function.

Data collection and preprocessing. In six subjects, iEEG signals were acquired continuously at 3 kHz per channel (16-bit precision, range ±8 mV, DC) with a Tucker Davis PZ5M data acquisition module (Tucker Davis Technologies, Alachua, FL). In the other two subjects, a standard clinical recording system (XTELK EMU 256 LTM System; Natus Medical) was used, sampling at 512 Hz. iEEG data from both systems were extracted similarly by bandpass filtering (8-pole Butterworth filter, cutoffs at 0.01 and 300 Hz), and similar results were obtained across systems. Either subdural or skull electrodes were used as references, as dictated by recording quality at the bedside, and were subsequently re-referenced to a common average to ensure consistency across participants and to reduce line noise. We inspected the power spectrum of the signals online before the start of the experiment to ensure its physiological properties.

The breathing cycle was assessed simultaneously by configuring a custom piezoelectric manometer within a nasal cannula device and recorded with the iEEG record for subsequent offline analysis. Subjects were not informed of the purpose of the cannula (i.e., they were simply asked to place it in the correct position before the start of the study). After the subjects firmly fixed the device in place, a 3-min period was allowed to get accustomed to wearing it. In the breath-counting experiments, the natural breathing blocks were run before the breath-counting blocks, to ensure that subjects did not attend to their breath more than usual during the natural breathing condition.

Experimental tasks. In the natural breathing experiment (see Figs. 2–6), subjects were instructed to rest wakefully (with their eyes open) during an 8.5-min period. We refer to natural breathing as the spontaneous or autonomic breathing of the subject when no cognitive task is performed. In the volitional breathing experiment (see Fig. 8), subjects were asked to slightly increase their nasal breathing rate from natural breathing. Subjects alternated between 2.5-min blocks of natural breathing and faster breathing (8 blocks total, 4 in each condition). We discarded the first 30 s of each block from the analysis, because the breathing rate usually became more regular after that initial period. Respiration signals were smoothed with a moving average filter and DC offset-corrected using standard MATLAB functions ("smooth.m" with a 10-point moving average window, and "detrend.m," respectively). All blocks were visually inspected, and those with unstable respiration signals (e.g., containing low signal-to-noise ratio or brief periods of absent signal due to mouth respiration) were discarded. Remaining blocks were concatenated within each condition before coherence analysis (8-min total per condition). In the attention-to-breath (interoceptive) experiment (see Figs. 9 and 10), subjects were asked to count their breaths for periods of 2 min (8 blocks total), reporting their counts after each period (Levinson et al. 2014). A 30-s resting interval was given between blocks. Accurately reported blocks, where subjects correctly reported the number of breaths within ±1 breath, were compared with inaccurately reported blocks. The experiment was continued until four blocks of each condition (correct and incorrect) were collected. In total, subjects completed 36 correct blocks (median = 6, range = 5–7) and 25 incorrect blocks (median = 4, range = 4–5). In the attention-to-external-stimuli (exteroceptive) experiment (see Fig. 10*A*), a task adapted from sustained attention and vigilance paradigms was used (Greicius et al. 2003; Kajimura and Nomura 2015, Leth-Steensen et al. 2000). Subjects viewed a screen containing four circles at different fixed locations while wearing the spirometry apparatus. After 10 s, the center of a randomly assigned circle turned from black to white. Subjects were asked to press one of four corresponding keyboard keys to indicate which circle filled, as quickly and accurately as possible.

Coherence and power analysis. To calculate coherence between the iEEG and the breathing signals (iEEG-breath coherence), we computed the cross-spectrum. The magnitude of the cross-spectrum was squared, normalized by the power spectra of each signal at each respective frequency, and smoothed (Mitra and Pesaran 1999). Each 8-min data set was divided into overlapping 32-s windows (1/32 = 0.03-Hz resolution, sliding 5 s at a time). Statistical significance was evaluated by creating surrogate trials. The iEEG signal was shuffled with respect to the breathing signal (1,000 iterations) by circularly shifting the signals through consecutive random displacements, and the critical levels of the pointwise Wilcoxon-Mann-Whitney tests at each frequency were computed (see dashed magenta lines in Figs. 2*C* and 8*A*; $\alpha = 0.01$). To calculate the breathing rate, the instantaneous frequency of the breathing signal was computed using a short-time Fourier transform. Computing the breathing rate by averaging the time between peaks in inhalation rate gave similar results. To ensure that the breathing signal was as stationary as possible, we excluded the initial 30 s from each block, because breathing rates usually stabilized within that time. All included breathing segments were also visually inspected to ensure signal quality. After computing iEEG-breath coherence values for all frequencies, we extracted the coherence value at the respiratory rate (see dashed green lines in Fig. 2*C*). Only the peak coherence at the respiratory rate was considered for further analysis. Coherence values at frequencies different from the respiratory rate were not considered in this study because breath manometry transduction is nonlinear, and higher-order components of the resultant signal (e.g., harmonics of the respiration signal and other mechanical artifacts that may appear in its power spectrum) are not necessarily reflective of physiological properties of the breath. For comparison, we also calculated coherence values with other methods, such as use of the wavelet transform ("globalcoher.m" function in MATLAB; The MathWorks, Natick, MA) and multitaper ("coherency.m" function in the Chronux toolbox; Mitra and Pesaran 1999). The results were nearly identical (data not shown). To determine the significance threshold for coherence among electrodes (e.g., see dark gray area in Fig. 3*B*), we used the 99% confidence interval (upper bound) of the averaged shuffled coherence across electrodes. Other methods to calculate a significance threshold (e.g., using the *P*-value method derived from the real data, which was well fitted by a bimodal distribution, $P < 0.05$, Hartigan's significance test) yielded similar results.

The critical value in Fig. 8*C* (thick red line) was calculated with bootstrapping statistics. First, iEEG and breathing signals for each electrode and condition (breathe normally vs. faster) were randomly shuffled (1,000 iterations). Second, coherence values were calculated for each iteration and then averaged to give rise to a surrogate distribution. The red line represents the 95th percentile of the median of the surrogate data after smoothing with a window size of 0.1 Hz and a slide of 0.01 Hz. The time-frequency coherence spectrum between the respiration and iEEG signals (see Fig. 8*B*) was computed using wavelets. To compute the difference in coherence values between breath-count correct and incorrect blocks (see Fig. 9*B*), we subtracted the coherence at the respiratory rate in the incorrect blocks from that in the correct blocks for each electrode and then normalized by their sum for each subject separately (see Fig. 9*C*). This normalization procedure was done to eliminate differences in overall coherence across subjects. To compare the alpha power between breath-count correct and incorrect blocks (see Fig. 9*A*, *inset*) alpha oscillations were extracted from the raw iEEG by bandpass filtering each 8-min data block between 8 and 13 Hz [150th-order finite impulse response (FIR) filter]. The instantaneous alpha-band amplitude was defined as the absolute value of the Hilbert transform of this signal. Data from each electrode were normalized (the difference in alpha power between conditions was divided by their sum), and the resultant distributions were compared using a Wilcoxon signed-rank test with a 95% confidence interval.

In the exteroceptive attention task (see Fig. 10*A*), subjects completed 48 trials (~9 min, depending on reaction time). Coherence values were calculated as for the experiments described above. The initial and final ~30-s segments were removed so that data windows

were identical in length (8 min) across breathing conditions (exteroceptive-attention, breath-count correct and incorrect). Resultant coherence values from each condition were normalized by subtracting the coherence from the natural breathing condition and dividing it by its sum [e.g., (breath-count correct − natural)/(breath-count correct + natural)]. Normalized coherence values were subjected to Kruskal-Wallis ANOVA test and subsequent post hoc Tukey's test comparisons (95% confidence interval). To determine if iEEG-breath coherence was affected by reaction time (see Fig. 10*C*), time-frequency coherence spectrograms were computed for the entire data set (~9 min, 48 trials) using wavelets. Single-trial iEEG-breath coherence values were extracted from the time windows and frequencies of interest (e.g., the 0–10 s before the subject's response at the respiratory frequency) for each electrode and plotted as a function of reaction time. Correlation and *P* values for Spearman's ρ were computed using the exact permutation distributions.

To estimate differences in breathing rate across conditions (see Fig. 10*F*, *bottom*), the intervals between peaks of inhalation rate were measured and the resultant distributions compared using Wilcoxon rank sum tests with a 99% confidence interval. The same criterion was used for estimating differences in breathing amplitude across conditions, after the peaks of the respiratory signal were measured.

Phase-amplitude coupling analysis. To find, across all the brain regions sampled, those with relatively locally generated respiration-related oscillations, gamma oscillations were extracted from the raw iEEG by bandpass filtering the raw iEEG data between 40 and 150 Hz (zero phase distortion and 150th-order FIR filter). The instantaneous amplitude of gamma was defined as the absolute value of the analytic signal as obtained by the Hilbert transform. To examine the coupling of the gamma amplitude to the breathing signal, the instantaneous phase of the breathing signal was extracted (angle value of the analytic signal) and binned in 18 segments (see Fig. 5*B*). For each of these segments (or phase bins), we measured the corresponding gamma amplitudes and normalized the result using a modulation index (Tort et al. 2008). The resultant modulation index (MI) values were compared against surrogate MI values, which were obtained by shuffling the respiration phases with respect to their gamma amplitudes. By repeating the shuffling process 1,000 times, we could infer a MI chance distribution and obtain a significance threshold ($P < 0.01$) by calculating the proportion of surrogate MIs greater than real MIs. To determine the significance threshold for coherence among electrodes (see dark gray area in Fig. 5*D*), we used the 99% confidence interval (upper bound) of the averaged shuffled coherence across electrodes.

Coupling of the respiratory phase to the gamma-band amplitude has previously been shown as a good indicator of intrinsic network activity (Ito et al. 2014). In turn, coupling of the respiratory phase to the lower frequency bands (e.g., theta) can also reveal intrinsic local influences in specific brain regions (Zelano et al. 2016), but it is generally more heterogeneous across brain regions and subjects (Heck DH, McAfee SS, Liu Y, Babajani-Feremi A, Rezaie R, Freeman WJ, Wheless JW, Papanicolaou AC, Ruszinko M, Kozma R, unpublished observations; Heck et al. 2017) and can be more susceptible to distal influences (Lakatos et al. 2005). Because of these reasons, frequency coupling of beta and theta oscillations was not analyzed in this study.

Electrode localization. Electrode positions were mapped to brain anatomy using registration of the postimplantation computed tomography (CT) to the preimplantation MRI via the postoperative MRI (Groppe et al. 2017). The CT was first coregistered with the postimplantation structural MRI and subsequently, with the preimplantation MRI. The coregistration was done with automated alignment software using FSL's FLIRT (Jenkinson and Smith 2001; Jenkinson et al. 2002; Mehta and Klein 2010). These transformation matrices were concatenated to register the CT to the preimplant MRI, thus accounting for the possibility of brain shift following implant surgery. After coregistration, electrodes were identified on the postimplantation CT scan using BioImage Suite (Papademetris et al. 2006), and subdural grid and strip electrodes were snapped to the closest point on the reconstructed brain surface (Dale et al. 1999) of the preimplantation MRI using MATLAB (Dykstra et al. 2012; Groppe et al. 2017). We then used the FreeSurfer automated parcellation (Fischl et al. 2004) to identify the anatomical region in which each electrode contact was located (Table 1), within ~3-mm resolution (the maximum parcellation error of a given electrode to a parcellated area was <5 voxels/mm). This parcellation method also localizes electrodes with respect to gray matter, white matter, and CSF with the same resolution. Electrodes with parcellation errors ≥5 voxels were excluded from the analysis. Due to lack of specificity of the FreeSurfer parcellation in the ventral aspect of the frontal lobe (Klein et al. 2017), we visually inspected the coregistration of each electrode assigned to the orbitofrontal cortex (medial portion, $n = 55$; lateral portion, $n = 25$) and the pars orbitalis ($n = 9$) using the patient's coregistered postimplantation MRI. From these, we identified 10 electrodes in the olfactory bulb and 9 in the piriform cortex. Verifying these localizations, high-frequency electrical stimulation of electrodes in the olfactory bulb resulted in perceptual report of a specific odor (2 patients reported a burning smell, 1 patient chlorine, and another perfume) during routine clinical functional mapping. Related MRI images were closely inspected and showed that the electrodes were sitting on top of the cribriform plate of the ethmoid bone (see Fig. 5*A*). No lasting postoperative damage to olfactory perception was reported by any of the patients, which was expected given the smaller size of the electrodes compared with total olfactory bulb volume.

For visualization on the brain surface, electrodes were snapped to the nearest point on the FreeSurfer pial surface and plotted on the inflated brain. Electrodes were excluded from analysis if they lay within 5 mm from the pial surface in any direction (*x*, *y*, or *z*). To coregister depth electrodes to an average brain (FreeSurfer's fsaverage), we used an affine transform to MNI305 space. To coregister surface electrodes, we used the method described by Dykstra et al. (2012) and implemented in the iElVis toolbox (Groppe et al. 2017): the patient's pial surface was warped to a sphere that FreeSurfer has gyrally aligned to a sphere version of the average brain's pial surface (Dale et al. 1999; Fischl et al. 2004). Each point on the patient's spherical surface was assigned to the nearest neighbor on the average brain spherical surface, in which each vertex corresponds to a vertex on the average brain pial surface.

Figure 1*A* shows the CT scout of a typical sEEG implant, where iEEG signals were recorded from 231 contacts that lay outside the seizure onset zone. The number of contacts implanted per patient typically ranged from 100 to 250. Platinum sEEG electrode arrays were used in five patients (e.g., Fig. 1*A*), and subdural strips and a grid were used in one patient (Fig. 1*B*). sEEG electrode arrays ranged from 8 to 16 intracranial contacts with 2.25 to 4.5-mm intercontact spacing, and grid and strip arrays were 1–3 mm in diameter with 4- to 10-mm center-to-center intercontact spacing.

RESULTS

Electrode sampling and task. Simultaneous recordings of iEEG and respiration were performed in six patients with medically refractory epilepsy. Patients were implanted with either sEEG depth (Fig. 1*A*) or subdural electrocorticography (ECoG) grids and strip arrays (Fig. 1*B*), and wore a custom spirometer attached to a nasal cannula to track their natural breathing cycle during an 8.5-min period. iEEG from a total of 1,137 electrode sites spanning deep and superficial brain areas were analyzed. Electrodes with epileptiform discharges were excluded from the analysis (see MATERIALS AND METHODS). Electrode sites were transformed to Desikan-Killiany parcellation space using custom scripts (Groppe et al. 2017). Table 1 shows the electrode locations and the sampling across different

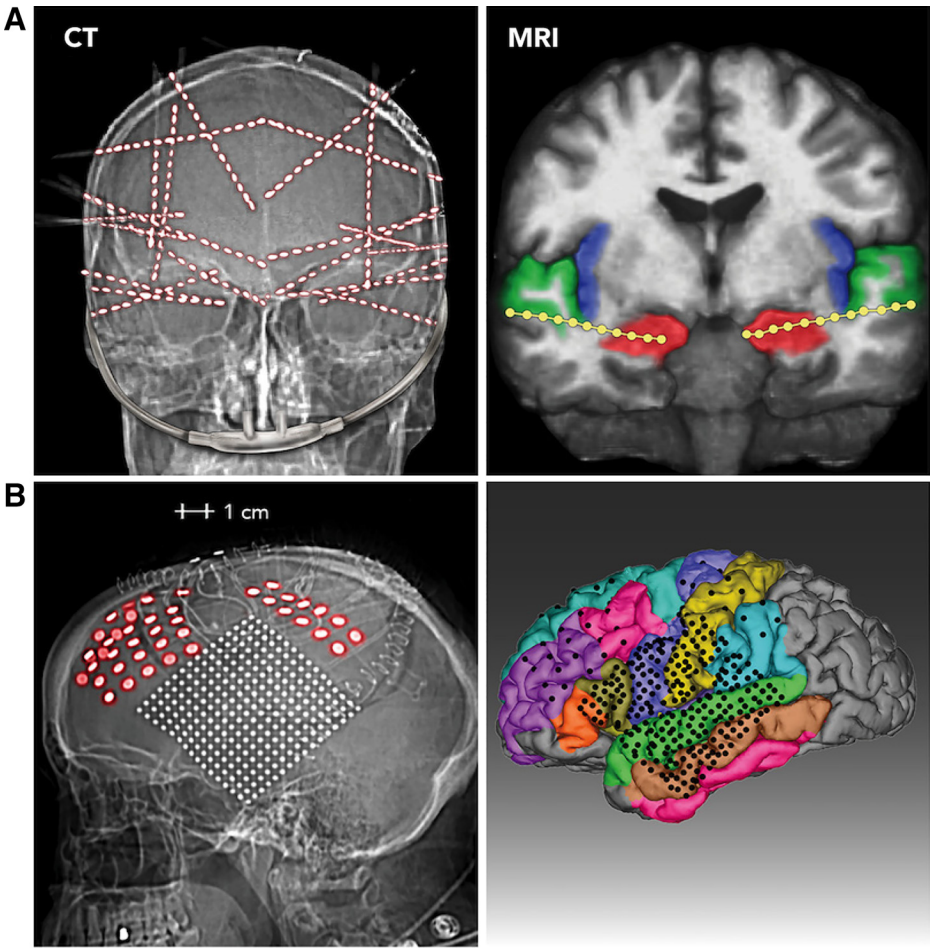

Fig. 1. Electrode localization in 2 representative patients. Two methods of electrode survey are used. *A*: CT (*left*). Postoperative skull radiograph is from 1 subject implanted with 20 stereo-depth EEG (sEEG) electrode arrays. Of the 320 contacts implanted in this subject, 231 were analyzed for breathing-related activity because they were outside the seizure onset zone and provided artifact-free signals. *Right*, MRI image of the same patient, showing 2 electrode arrays with the deepest contacts (1–4) in the hippocampi (red), superficial electrodes in the superior temporal gyrus (green), and a number of intervening electrodes lying in the white matter. *B*: CT (*left*). Lateral view of head radiograph is from the 1 subject who was implanted with subdural ECoG grids and strips. *Right*, MRI reconstruction showing the location of the electrodes on a parcellated brain (FreeSurfer; Dale et al. 1999; Fischl et al. 1999).

regions of gray matter ($n = 809$), white matter ($n = 318$), and CSF ($n = 10$).

Brain areas demonstrating coherence with breathing. Rodent studies have shown the hippocampus (Nguyen Chi et al. 2016; Tsanov et al. 2014) and somatosensory cortex (Ito et al. 2014) exhibit respiration-locked oscillations. To test for a similar effect in humans, we measured the phase locking between the iEEG and the breathing cycle (iEEG-breath coherence) for each electrode that was outside the SOZ ($n = 1137$, 6 subjects). Subjects were asked to breathe naturally during an 8.5-min period. A sample spirometry trace (black line) and simultaneous iEEG signal (red line) from a single electrode in the hippocampus of one subject are shown in Fig. 2*A*, *top*, demonstrating an example in which low-frequency oscillations are strongly synchronized to the breathing cycle (coherence value coh = 0.62, $P = 0.0001$; Fig. 2*C*, *bottom*). In contrast, an electrode located ~1 cm away in the adjacent white matter (Fig. 2*A*, *bottom*) showed no peak near the breathing rate in the iEEG trace spectrum, and a much smaller coherence value there (coh = 0.02, $P = 0.44$; Fig. 2*C*, *bottom*).

Across the data set (Fig. 3*A*), 33% (374/1,137) of the sites analyzed showed high (>99th percentile of the surrogate distribution threshold) coherence values at the breathing rate. Eighty-nine percent of sites demonstrating high coherence (334/374) were located in the gray matter, 11% were in the white matter (40/374), and none were in CSF. Sites in gray matter had higher likelihood of demonstrating high coherence: 41.3% of the total sites in the gray matter (334/809) showed coherence above threshold compared with 12.6% of the total sites in the white matter (40/318) (Fig. 3*A*). Furthermore, coherence values were lower in white matter and CSF compared with gray matter (Fig. 3*B*; $P < 0.001$, Wilcoxon rank sum test, both comparisons). We tested for the presence of two populations of gray matter sites, one of which tracks the breathing cycle and the other that does not. Coherence values in the gray matter were well fitted by a bimodal distribution ($P < 0.05$, Hartigan's significance test) with two local modes at 0.12 and 0.25.

The greater likelihood of iEEG-breath coherence in gray matter and the stronger iEEG-breath coherence values observed indicate that the observed coherence in the iEEG signal is related to neuronal activity rather than artifact from nonneural signals related to breathing (Cardoso et al. 1983; Urigüen and Garcia-Zapirain, 2015). Within the gray matter, electrodes with large coherence values (>99% percentile of the surrogate data) were distributed across a variety of areas (Fig. 4*A*), including the parietal, sensorimotor, premotor, prefrontal, cingulate, insular, and visual cortex as well as in the hippocampus, amygdala, and primary olfactory cortex. These results provide important controls and complement recent reports correlating breathing and cortical iEEG in humans (Heck DH, McAfee SS, Liu Y, Babajani-Feremi A, Rezaie R, Freeman WJ, Wheless JW, Papanicolaou AC, Ruszinko M, Kozma R, unpublished observations; Heck et al. 2017; Zelano et al. 2016).

Local generators of respiration-locked oscillations. We next sought to examine the relationship between iEEG oscillations

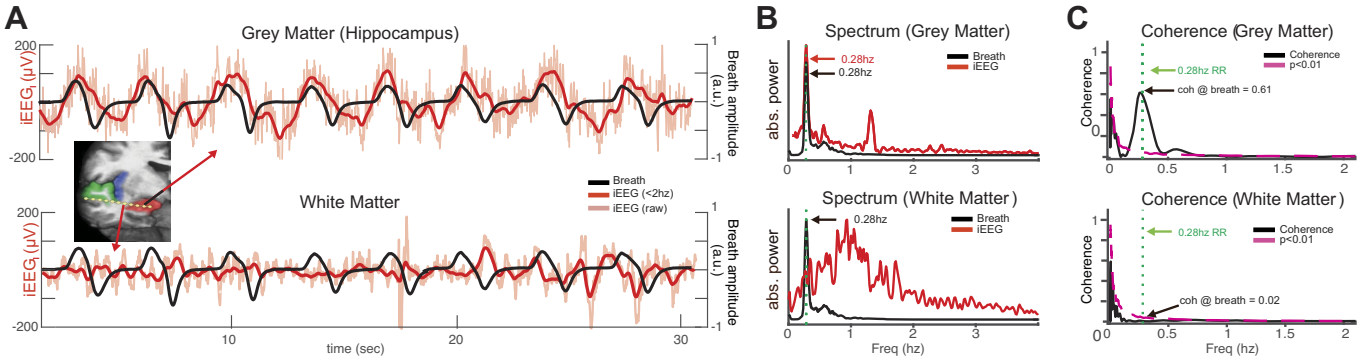

Fig. 2. Coherence between the intracranial EEG (iEEG) and the breathing during natural respiration. *A*: iEEG (red lines) and breathing signals (black lines) during a representative 30-s period during natural respiration for 2 sample electrodes: one in the hippocampus (*top*), which shows strong phase-locked signals, and another in the white matter (*bottom*) showing negligible phase locking. *B*, *top*: power spectrum of the manometric breathing signal (black line) and the hippocampal iEEG trace (red line), both with peaks at 0.28 Hz. The iEEG shows an additional peak at 1.33 Hz. *Bottom*, power spectrum for an electrode in the adjacent white matter showing no such peak at the breathing rate. *C*, *top*: coherence between respiration and hippocampal signals. The coherence value at the 0.28-Hz respiratory rate (dashed green lines) was significant (coherence value = 0.62, $P = 0.0001$). Significance (magenta dash line) was evaluated by performing bootstrap analysis shuffling iEEG and breathing signals (1,000 iterations, $P < 0.01$). *Bottom*: iEEG-breath coherence from an electrode in the white matter. The coherence value at the breathing frequency (dashed green line) was not significant (coherence value = 0.02, $P = 0.44$). abs., Absolute; a.u., arbitrary units; RR, respiratory rate.

and local neuronal activity. Whereas iEEG oscillations may reflect both propagated activity and intrinsic rhythms (Kajikawa and Schroeder 2011; König et al. 1996; Łęski et al. 2013), local broadband gamma power is thought to represent locally generated neuronal activity (Miller et al. 2007a, 2012; Zhang et al. 2015). By examining the coupling of broadband (40–150 Hz) gamma power to the respiratory cycle, we demonstrate phase locking of broadband gamma to specific phases of the breathing cycle. A sample site is shown in Fig. 5*A*: an electrode touching the olfactory bulb exhibits gamma amplitude increases at specific phases of the breathing cycle. We quantified this relationship by measuring the gamma amplitude at each phase bin of the breathing cycle and calculating a modulation index (MI) (Tort et al. 2008; Tort AB, Ponsel S, Jessberger J, Yanovsky Y, Brankačk J, Draguhn A, unpublished observations). The distribution of the observed phases for this site is not flat (Fig. 5*B*), unlike the surrogate distribution, demonstrating a significant MI at specific phases of the breathing cycle (MI = 0.52, post hoc Tukey's test, $P = 0.0005$).

Across the population data (Fig. 5*C*), high MIs were observed in 138/1,137 sites (12.2%, >99th percentile of the surrogate distribution). Nearly all of these sites (136/138) also had strong iEEG-breath coherence in the analysis shown above. The two sites with coherence but no CFC were located in the hippocampus and the insula. As expected, MIs were smaller in the white matter and CSF compared with the gray matter (Fig. 5*D*; $P = 0.0001$, Wilcoxon rank sum test), and no electrode in white matter or CSF showed a significant MI. Greater than 37% of electrodes in the insula, amygdala, hippocampus, pars orbitalis, and motor, parietal, and primary olfactory cortices showed high MIs above the threshold (Fig. 5*E*). High MIs were also demonstrated across a number of other areas, including the temporal, cingulate, lingual, and

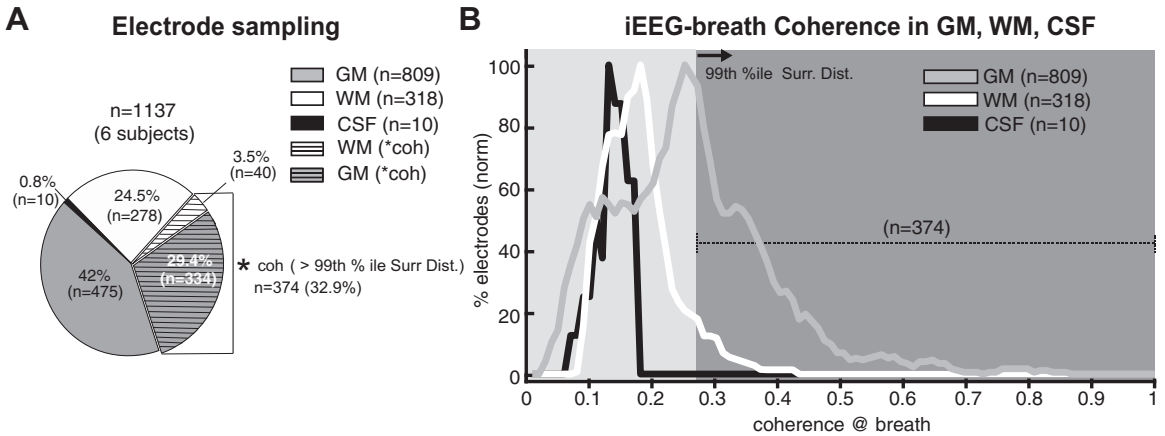

Fig. 3. *A*: iEEG-breath coherence in gray matter (GM), white matter (WM), and cerebrospinal fluid (CSF). Pie chart shows the total number of electrodes (n = 1,137 in 6 subjects) and the electrodes that showed iEEG-breath coherence greater than 99th percentile of the surrogate distribution derived from shifting the respiration signal with respect to the iEEG [asterisk indicates coherence >99% percentile; n = 374 (32.9%), horizontal hatching]. Most of the electrodes with greater coherence were in gray matter. *B*: distribution of coherence values at the respiratory rate across the population of GM, WM, and CSF electrodes as a percentage of the total of each. Coherence values were larger in most electrodes located in the GM than those in WM and CSF. Values (y-axis) were smoothed (0.02 window width) before being plotted and are normalized (norm) for each area (GM, WM, or CSF) separately. Dark gray area shows coherence greater than 99th percentile (n = 374). GM sites show a bimodal distribution, with one population showing higher local mode at 0.25 and the other at a mode close to that of the WM and CSF at 0.12. coh, Coherence value; 99% ile Surr Dist., >99th percentile of the surrogate distribution.

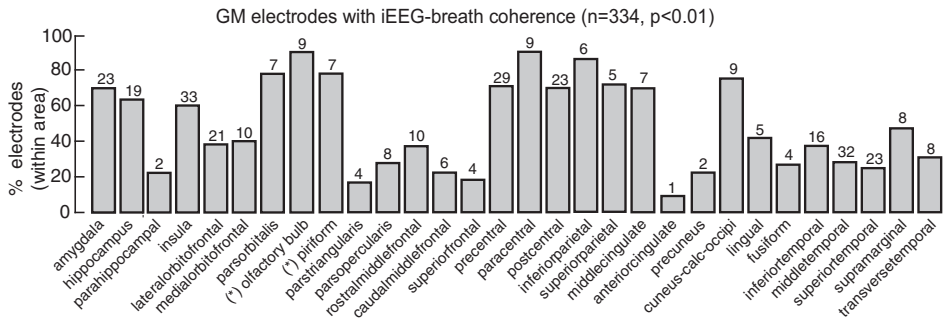

Fig. 4. Percentage of gray matter electrodes within each brain area showing iEEG-breath coherence above the threshold (99th percentile). Numbers above each bar represent the total number of electrodes within that area showing the effect. Asterisks indicate electrode locations after correction using FreeSurfer parcellation (see MATERIALS AND METHODS). Cuneus-calc-occipi, cuneus-calcarine-occipital.

occipital cortices. This gamma phase locking to breathing cycle and the specificity of the effect in the gray matter also provide further evidence of the nonartifactual nature of this measured response.

The specificity of the observed effects in gray matter (and not white matter and/or CSF) was seen across subjects. Figure 6 shows consistent iEEG-breath coherence and cross-frequency coupling across subjects. A summary of the effects localized on an inflated brain surface is shown for a representative subject (Fig. 7*A*) and across the population of subjects ($n = 6$; Fig. 7*B*) localized on a common inflated surface (see MATERIALS AND METHODS). Effects are widely distributed across brain areas.

Volitional control of breathing. One major advantage of breathing-related research with human subjects is their ability to follow simple instructions regarding their breathing. To understand the effects of volitional control of breathing on iEEG-breath coherence, we asked our subjects to breathe faster than usual and measured the respiration-locked oscillations in their iEEG signals (iEEG-breath coherence). We hypothesized that iEEG-breath coherence would increase in those areas involved in voluntary pacing of breathing. As can be seen from a representative electrode in the frontal cortex and the simultaneously recorded breathing signal (Fig. 8*A*), phase locking decreases as the subject gradually transitions from an intentionally faster breathing to a more natural automatic breathing. The time-frequency coherence spectrum between these signals (Fig. 8*B*) shows that the frequency at which coherence is greatest, as well as the magnitude of that peak coherence, decreases as the subject breathes more slowly. Across the sample of gray matter sites ($n = 809$; Fig. 8*C*), coherence values at the breathing rate were increased during fast breath-

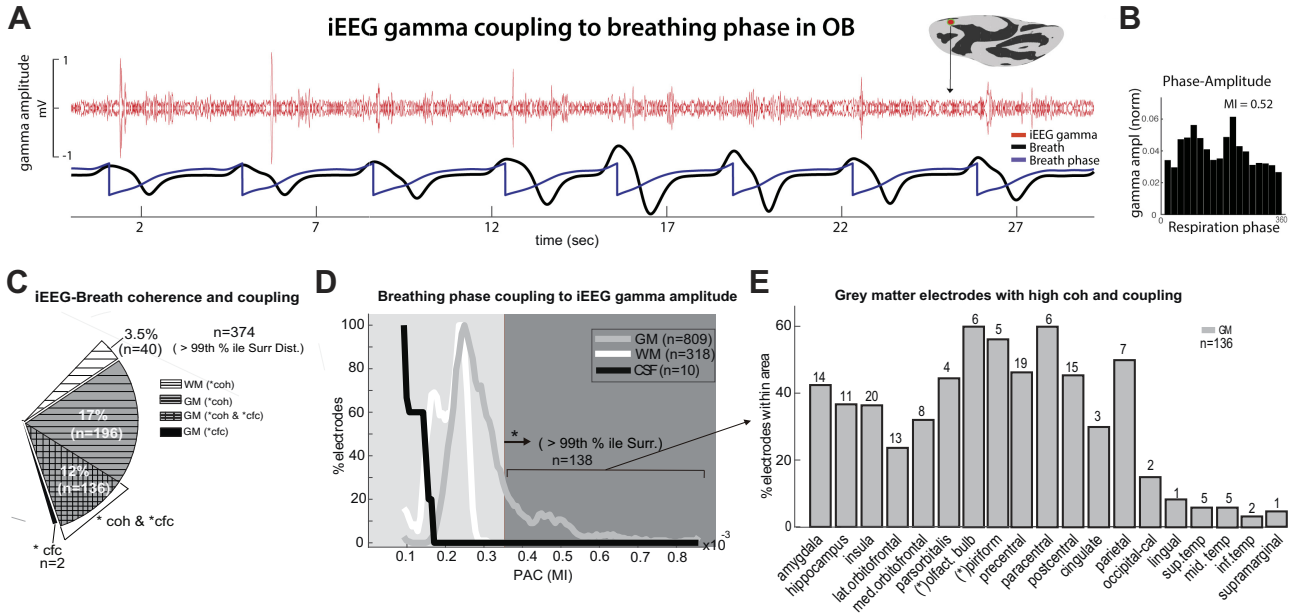

Fig. 5. Breathing-phase coupling to gamma-amplitude oscillations. *A*: sample electrode in the olfactory bulb (OB) exhibiting bursts of broadband signal (40–150 Hz) at specific phases of the respiratory cycle, particularly during the beginning and end of exhalation during natural breathing. *B*: gamma-band amplitude at different phases of the breathing signal (18 bins of 20° width each) for this sample electrode averaged across an 8-min period. *C*: iEEG-breath coherence and cross-frequency coupling in GM, WM, and CSF. Pie chart shows the percentage of electrodes exhibiting large coherence values (>99th percentile; horizontal hatching) as well as cross-frequency coupling (cross-hatching), and cross-frequency coupling alone (black) across the population ($n = 1,137$ electrodes). *D*: distribution of modulation indexes (MIs) across the population of GM, WM, and CSF electrodes. Lines represent raw MIs after smoothing (window width = 0.02). MIs were smaller in electrodes located in the CSF and WM compared with electrodes in the GM. Only 138/1,137 (12.2%) of the electrodes showed MIs above the threshold, all located in the GM. The threshold (dark gray area) was the 99th percentile of the surrogate MI distribution derived from shifting the respiration signal with respect to the iEEG (as indicated by asterisk). The *y*-axis represents electrode percentages normalized with respect to each area (GM, WM, and CSF), separately. *E*: percentage of GM electrodes within each brain area that showed both MIs and coherence values above the threshold. Up to 40% of the electrodes that were in the amygdala, hippocampus, insula, motor, parietal, and primary olfactory cortices showed increased gamma-amplitude oscillations at specific phases of the respiratory cycle. cfc, cross-frequency coupling; coh, coherence; PAC, phase-amplitude coupling; lat., lateral; med., medial; olfact., olfactory; occipital-cal, occipital-calcarine; sup. temp, superior temporal; mid. temp, middle temporal; inf, inferior.

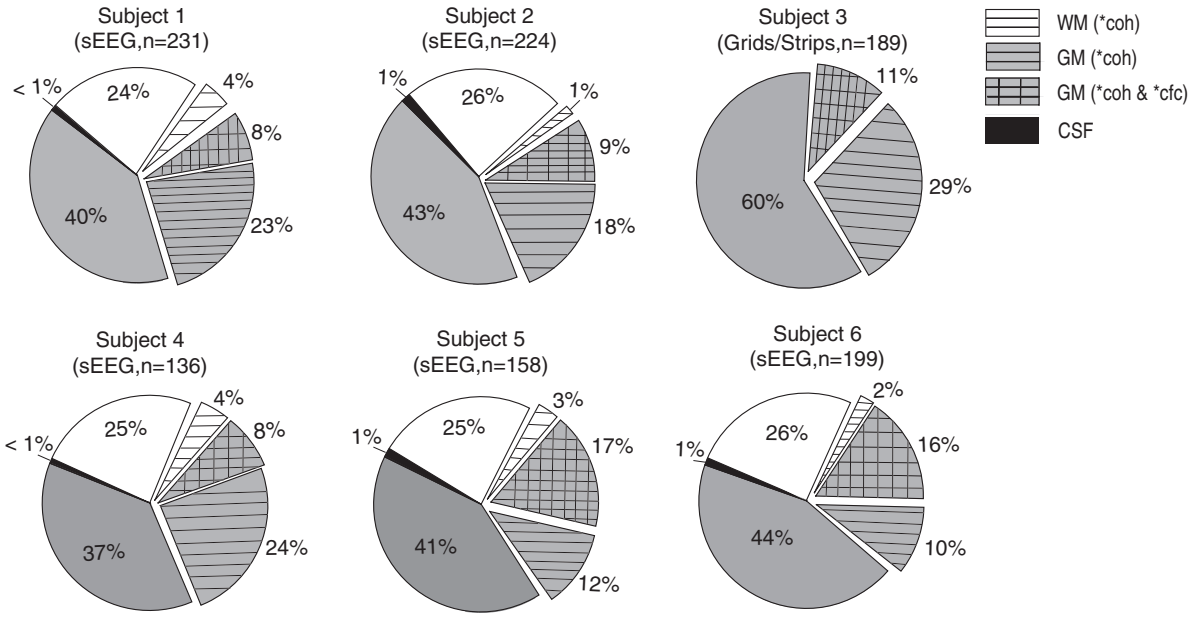

Fig. 6. Electrode sampling and effects in 6 individual subjects (n = total number of electrodes analyzed in each subject after electrodes were removed from the SOZ). *Subject 3* was implanted with grids and strips and consequently had no electrodes in the WM or the CSF. The remaining subjects were implanted with depth (sEEG) electrodes. Each sEEG subject had electrodes implanted in the WM and the CSF. Pie charts show the percentage of electrodes with high iEEG-breath coherence (horizontal hatching; >99th percentile of surrogate distribution) and the percentage of electrodes with high iEEG-breath coherence as well as phase-gamma amplitude coupling (cross-hatching; >99th percentile). Only 2 electrodes showed high phase-amplitude coupling and low coherence (1 electrode in each of *subjects 1* and *2*; data not shown). coh, iEEG-breath coherence; cfc, cross-frequency coupling of iEEG-gamma amplitude to respiration phase. Asterisk indicates >99th percentile of the surrogate distribution.

ing compared with natural breathing ($P = 0.00011$, Wilcoxon signed-rank test). Electrodes with significantly larger coherence ($P < 0.05$, those above the red line in Fig. 8*C*, $n = 234$) were located in the frontal (caudal-medial, precentral, orbitofrontal, pars opercularis), insular, and superior temporal cortices and amygdala. Although these brain areas largely overlap with those showing coherence during natural breathing, the coherence is increased in magnitude during the intentionally fast breathing, particularly in precentral, lateral orbitofrontal, and insular cortices. In addition, there is recruitment of the caudal-medial frontal cortex during faster breathing, an area where activity is not coherent during natural breathing.

Interoceptive attention to breathing. Previous studies have shown that directing attention to external stimuli can improve sensory processing in cortical areas (Herrero et al. 2008; Lakatos et al. 2008; Mehta et al. 2000). However, little is known about how directing attention to internal bodily sensations, such as one's own breathing, modulates neuronal activity (Farb et al. 2013). We trained three of the above-described subjects each to direct their attention to their own breathing. To measure the degree of interoceptive attention to breathing, we asked these subjects to count the number of breaths and report the counts after multiple consecutive 2-min periods. The accuracy of the report can be used to gauge the degree of attention and has been used to track awareness during breathing exercises of meditative practice (Levinson et al. 2014). Across the data set of these subjects ($n = 355$ gray matter electrodes), correctly reported intervals showed larger iEEG-breath coherence compared with incorrectly reported ones (Fig. 9*A*; $P < 0.001$, Wilcoxon signed-rank test). Although overall coherence values varied across subjects, the effect was consistent within each subject individually (*subjects 4* and *5*, $P = 0.0013$; *subject 6*, $P = 0.014$, Wilcoxon signed-rank test). For *subjects 2* and *3*, a subset of electrodes showed significantly increased iEEG-breath coherence, most of which were distributed in the anterior cingulate, insular, and premotor cortices and in the hippocampus (Fig. 9, *B* and *C*). *Subject 1* showed significantly increased coherence in most electrodes, although the largest increases also occurred in the same brain areas (Fig. 9*C*).

Interoceptive attention or general arousal? Typically, incorrect reports were inaccurate by two to six breaths, and subjects reported momentarily losing their breaths counts for a few seconds before becoming aware of it and returning back to the count. However, to dissociate these effects from a possible reduction in arousal, power in the alpha (8–13 Hz) band was measured and compared between correctly and incorrectly counted trial blocks (Cantero et al. 1999; Klimesch et al. 1998). There were no significant differences in alpha power (Fig. 9*A*, *inset*) between correct and incorrect blocks for *subjects 5* and *6* ($P > 0.1$, Wilcoxon signed-rank test), although a trend was observed in *subject 4* ($P = 0.055$). This subject showed larger effect size compared with the other two subjects, with 118/123 electrodes showing larger coherence during correct reports.

Although alpha power did not differ across conditions in all subjects, suggesting comparable levels of arousal, we conducted an additional experiment in two of the subjects to rule out the possibility that the effect of attention to the breath is attributable to differences in general arousal. In this task (Fig. 10*A*), subjects were asked to direct their attention to a visual stimulus (e.g., exteroceptive attention, as opposed to interoceptive attention, as in attention to the breath). An example recording from an electrode located in the anterior cingulate cortex (Acc) is shown in Fig. 10*B*. Both subjects had electrodes implanted in the four regions of interest (*subjects 7* and *8*, respectively: Acc, $n = 3$ and $n = 4$; insula, $n = 12$ and $n = 15$;

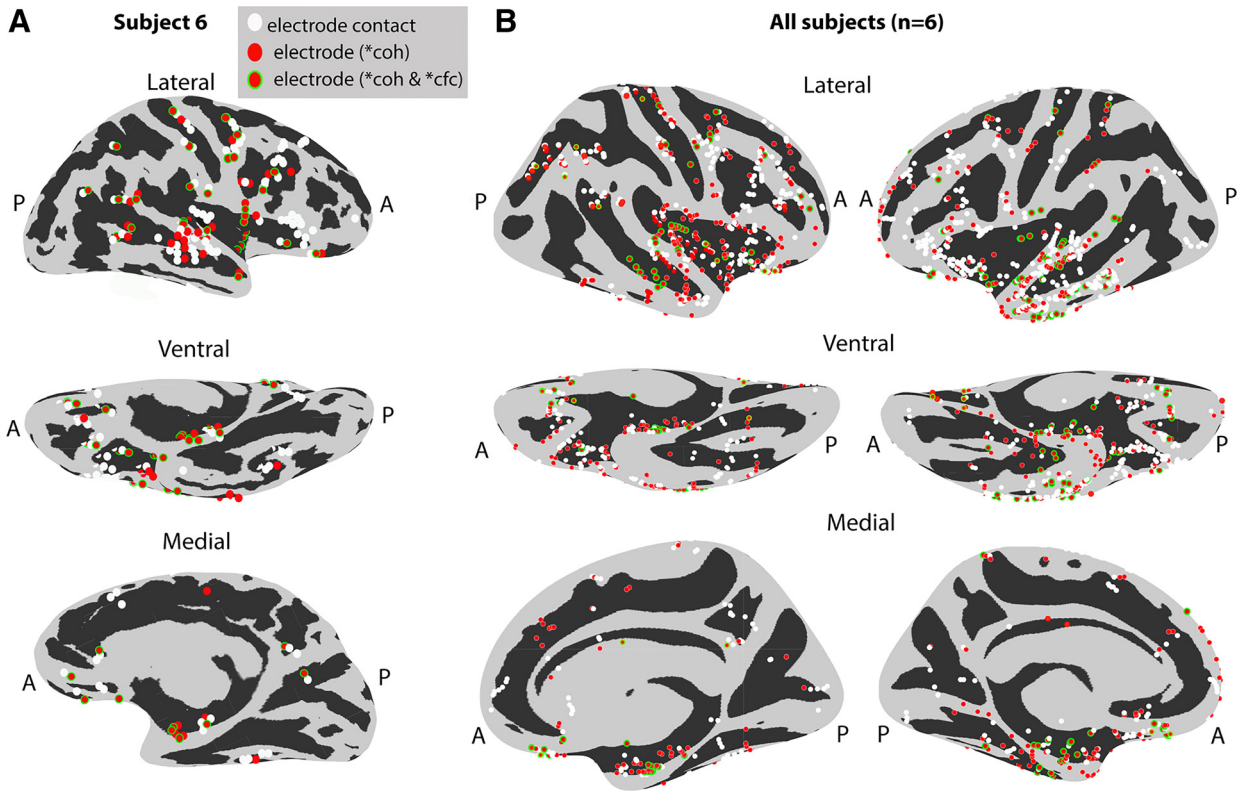

Fig. 7. Coherence and cross-frequency coupling effects localized on inflated brain surfaces. *A*: representative subject's inflated brain. Electrodes with high coherence (red) as well as cross-frequency coupling (red with green outline) are displayed in 3 different brain views (lateral, ventral, and medial). Other electrodes (white) had values below the 99th percentile threshold. *B*: electrodes from 6 subjects registered onto a common brain surface (see MATERIALS AND METHODS). Electrodes with high coherence and cross-frequency coupling are broadly distributed across multiple brain areas. A, anterior; P, posterior. Asterisk indicates >99th percentile of the surrogate distribution.

premotor, $n = 5$ and $n = 28$; and hippocampus, $n = 4$ and $n = 3$). They engaged in a task adapted from studies of exteroceptive attention (Leth-Steensen et al. 2000) that requires a state of continuous arousal while the iEEG-breath coherence was measured. We measured the level of arousal by testing the relationship between behavioral performance, as measured by reaction time, and iEEG-breath coherence (Fig. 10*C*). If arousal were to account for the findings shown in Fig. 10, a negative correlation would be expected in this analysis. Instead, there was a small positive correlation between these two variables in the Acc (*subject 7*: $r = 0.27$, $P = 0.0001$; *subject 8*, $r = 0.2$, $P = 0.017$) and no significant correlation in other areas.

Furthermore, iEEG-breath coherence at the respiration rate was higher during correctly reported intervals of breath counting (red lines) compared with incorrectly reported intervals (magenta) and exteroceptive attention intervals (black lines; Fig. 10*B*). At the population level ($n = 52$, Fig. 10, *C* and *D*), correct blocks showed larger coherence compared with both incorrect and exteroceptive blocks in Acc (post hoc Tukey's test, $P < 0.01$ and $P < 0.001$, respectively), insula ($P < 0.001$), premotor cortex ($P < 0.01$), and hippocampus ($P < 0.01$). Importantly, comparison between exteroceptive attention task and incorrect breathing count blocks did not show a significant difference in any of the four brain areas (post hoc Tukey's test, $P > 0.1$ for all brain areas). Additionally, intrasubject comparisons yielded no significant difference (Fig. 10*E*). These results further support the notion that the observed difference in iEEG-breath coherence between incorrectly and correctly counted trial blocks does not reflect arousal differences.

It is also unlikely that the observed interoception-dependent coherence dynamics reflect differences in breathing rate between conditions (Fig. 10*F*). Overall, respiration rates changed slightly across the different experimental conditions. Whereas respiration rates in *subject 7* decreased from 0.26 Hz during baseline (natural breathing) to 0.22, 0.21, and 0.22 during correct, incorrect, and exteroceptive breathing conditions, respectively ($P < 0.05$, Wilcoxon signed-rank test, for all comparisons), *subject 8* showed an opposed pattern with increased respiration rates from 0.26 Hz during baseline to 0.29 Hz during correct, incorrect, and exteroceptive breathing conditions ($P < 0.05$, Wilcoxon signed-rank test, for all comparisons). Thus, in both subjects (Fig. 10*C*, individual subjects), the iEEG-breath coherence change was independent of the direction of each subject's change in respiratory rate.

DISCUSSION

Whereas breathing has been traditionally thought of as an automatic process driven by the brain stem (Butler 2007; Foerster 1936; Tenney and Ou 1977), cortical and limbic involvement in breathing is increasingly being recognized (Aleksandrov et al. 2000; Biskamp et al. 2017; Ito et al. 2014; Tsanov et al. 2014). In the present study, we demonstrate respiration-locked oscillations in the human brain in cortical and limbic areas more widespread than shown previously and provide further evidence for the neuronal basis of these mea-

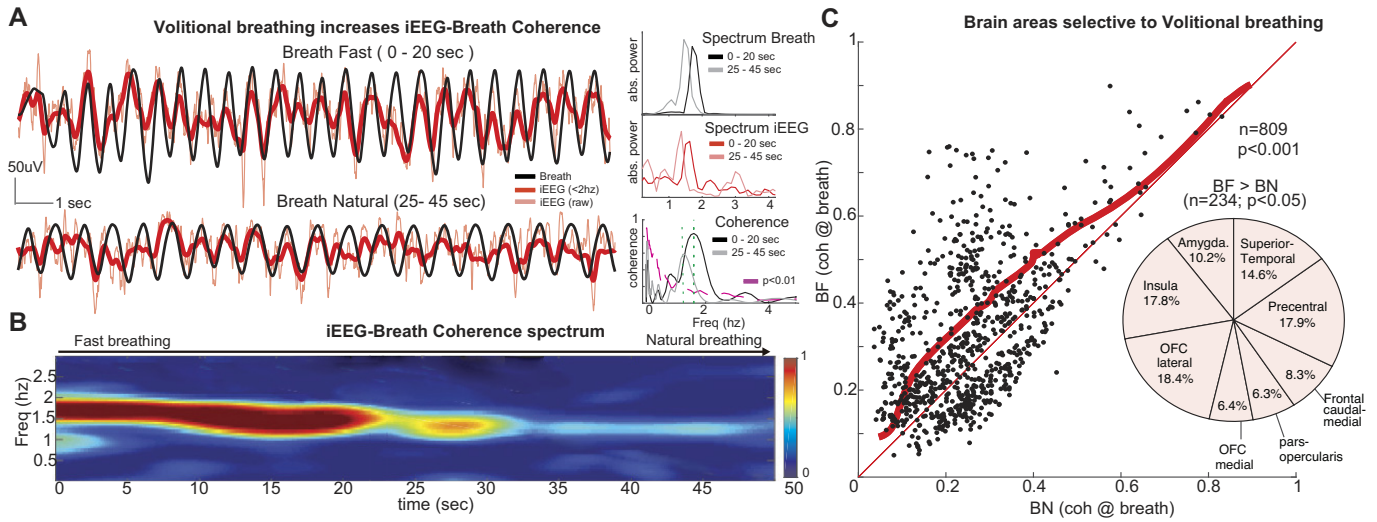

Fig. 8. Volitional breathing increases iEEG-breath coherence and recruits frontal networks. *A*, *left*: raw iEEG (red) and manometric respiration signals (black) from a sample electrode in the caudal medial frontal cortex during fast breathing (*top*; 0–20 s) followed by the transition to natural breathing (*bottom*; 25–45 s). Note the larger amplitude and faster frequency in both iEEG and breathing signals during the initial hyperventilation period, as well as the stronger iEEG-breath phase locking. *Right*, plots show the power spectrum peaks at 1.7 Hz during hyperventilation and at 1.4 Hz during transition to natural breathing for the respiration signal (*top*; black lines) and the iEEG signals (*middle*; red lines), as well as the iEEG-breath coherence (*bottom*). The coherence peak at the breathing rate (green dashed lines) is smaller when the subject breathes more slowly (gray line). *B*: time-frequency coherence spectrum between the signals shown in *A*. The peak in the spectrum closely follows the respiration rate. *C*: iEEG-breath coherence at the respiration rate for all electrodes in the gray matter (n = 809) during fast breathing (BF; vertical axis) and natural breathing (BN; horizontal axis). Coherence values were significantly increased across the population during fast breathing ($P < 0.001$, Wilcoxon signed-rank test). Thick red line shows the significance threshold ($P < 0.05$, bootstrapping method, 95% percentile) with 234/809 electrodes above the line showing significantly increased coherence values. Thin red line represents unity. Pie chart shows the locations of those 234 electrodes within the gray matter where coherence was significantly larger during fast breathing vs. natural breathing. Note the large proportion of electrodes in frontal areas, including caudal medial frontal cortex. Freq, frequency; OFC, orbitofrontal cortex.

surements by demonstrating gray matter (GM) specificity and cross-frequency coupling (CFC; coupling of the respiration phase to the gamma amplitude). The relevance of higher brain circuits to respiration-locked oscillations is highlighted by their sensitivity to cognitive factors such as volitional and attentive breathing. We further demonstrate that interoceptive attention to breath increases respiration-locked oscillations particularly in the anterior cingulate cortex, an effect that is distinct from general arousal.

Synchronization of neuronal activity to the breathing cycle. Because the breathing cycle is oscillatory, observed iEEG-breath coherence may be due to cyclical nonneural artifacts, such as intracranial pressure, cerebral perfusion, P_{O_2}, and P_{CO_2} (Brenner and Schaul 1990; Cardoso et al. 1983; Urigüen and Garcia-Zapirain 2015). However, these properties should be distributed throughout the intracranial space, with the more compliant and dynamically flowing CSF more prone to mechanical and chemical artifacts. Because depth electrodes often traverse white matter (WM) and CSF spaces as well as GM, it is possible to examine for GM specificity of the observed coherence. We demonstrated such coherence predominantly in GM (41.3%), rarely in WM (12.6%), and never in the CSF.

We also differentiate neuronal from nonneuronal signals by examining the coupling of high-frequency gamma-band activity to the phase of the observed low-frequency oscillation related to breathing. Similar to the case for coherence, GM specificity of effects supports a neuronal basis. We demonstrated phase-amplitude coupling of the breathing oscillation to the gamma band in a subset (12%) of sites (Fig. 5), with nearly all sites (136/138) also showing strong coherence. Respiratory modulation of intrinsic gamma network oscillations could be an organizing principle of cortical excitability, in line with recent hypotheses (Heck et al. 2017). Sites where coherence occurs without CFC (2/138) likely reflect propagated lower frequency modulatory inputs below action potential threshold (Kajikawa and Schroeder 2011; König et al. 1996).

Respiratory rhythm represents a fundamental and ubiquitous neuronal oscillation. Our results support and corroborate rodents studies demonstrating respiration-locked LFP and spike activity in the hippocampus (Nguyen Chi et al. 2016; Tsanov et al. 2014), barrel (Ito et al. 2014), and prefrontal cortices (Biskamp et al. 2017) and extend observations recorded from the rodent (Tort AB, Ponsel S, Jessberger J, Yanovsky Y, Brankačk J, Draguhn A, unpublished observations) and human brains (Heck DH, McAfee SS, Liu Y, Babajani-Feremi A, Rezaie R, Freeman WJ, Wheless JW, Papanicolaou AC, Ruszinko M, Kozma R, unpublished observations; Heck et al. 2017). In rodents, respiration is tightly coupled to olfaction (Welker 1964), as the respiration cycle strongly influences the information flow into the olfactory bulb (OB) and piriform cortex (Fontanini et al. 2003; Jiang et al. 2017; Kepecs et al. 2007). In the present study, we demonstrated respiration-locked oscillations in the OB, piriform cortex, and medial and lateral OFC (Fig. 5), extending such observations from the piriform cortex to humans (Jiang et al. 2017; Zelano et al. 2016). Furthermore, with widespread sampling, we demonstrated respiration-locked oscillations well beyond those structures and in 41% of the GM sites sampled (Fig. 3). Most consistent effects were recorded in the hippocampus, amygdala, insula, frontal, parietal, and primary olfactory cortices (Figs. 4 and 5*E*). Simultaneous recordings from the OB and the hippocampus in the mouse (Nguyen Chi et al. 2016) reveal that the OB drives the hippocampal respiration-rhythm and that theta oscillations in the OB are driven

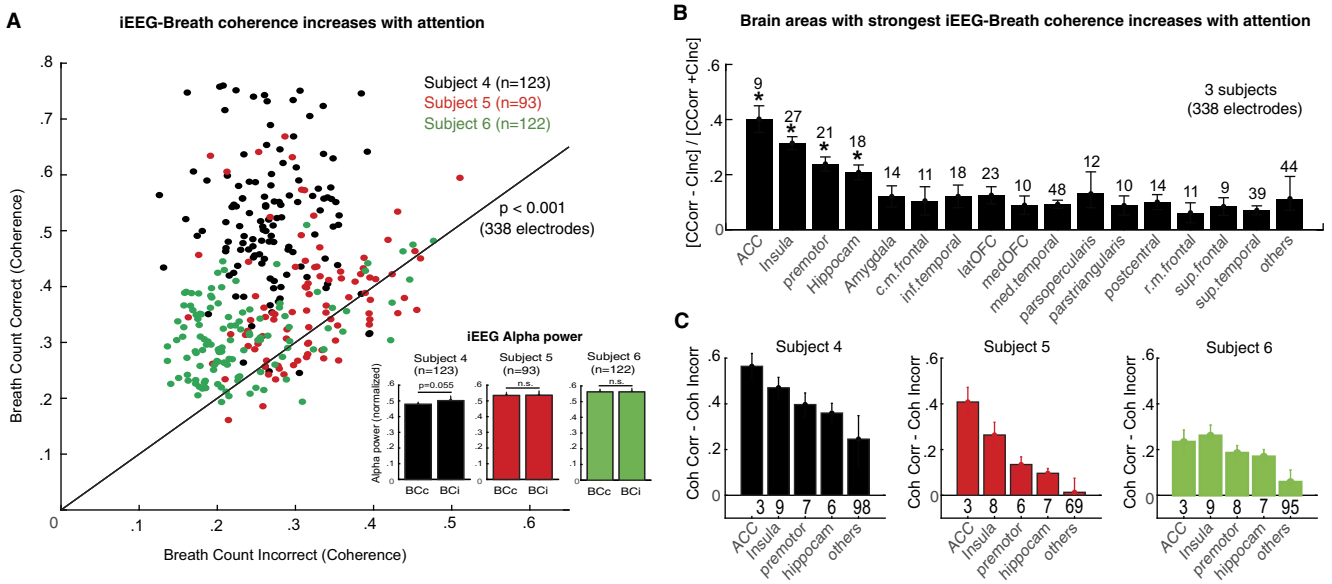

Fig. 9. Attention to breathing increases iEEG-breath coherence in brain areas related to interoception. *A*: iEEG-breath coherence values at the respiratory rate during correctly (*y*-axis) and incorrectly (*x*-axis) reported breath-counting periods across the population of gray matter electrodes ($n = 338$ in 3 subjects). Values were increased during correct periods in the 3 subjects collectively ($P < 0.001$, Wilcoxon's signed-rank test) and in each subject separately. Black line represents unity. *Inset*: normalized iEEG alpha power for the 2 conditions and 3 subjects averaged across electrodes sites. None of the subjects showed significant differences between correct and incorrect reports, although there was a trend in *subject 4* ($P = 0.055$) with slightly larger alpha power during incorrect reports. *B*: distribution of the effect across brain areas. Graph shows mean normalized differences in coherence between correctly and incorrectly reported counting periods. To normalize coherence values across subjects, the difference between correct and incorrect blocks for each subject was divided by their sum. Numbers above bars represent the total number of electrodes within the indicated area. *C*: coherence values in each subject and brain area (coherence correct – coherence incorrect). The strongest effect was observed in the anterior cingulate cortex, insula, premotor cortex, and hippocampus, and this pattern was consistent across subjects. Other brain areas showed smaller effects. $*P < 0.05$. Acc, anterior cingulate cortex. Bars indicate means, and error bars indicate SE.

by the hippocampus. In humans, breathing not only entrains higher frequency rhythms in the hippocampus, but the phase of respiration-related oscillations affects memory retrieval (Zelano et al. 2016). Our findings of breathing-related coherence in both OB and hippocampus corroborate previous findings, further establishing the connection between olfaction and memory (Jiang et al. 2017). Whereas in rodents, breathing is close to the theta rhythm, respiration-related oscillations have a frequency peak at ~3 Hz (during natural breathing) and appear to be clearly distinct from co-occurring theta (4–10 Hz) oscillations (Nguyen Chi et al. 2016). Given that the human correlate to rodent hippocampal theta is slower, at 1–4 Hz (Jacobs 2014), we also observed clearly distinct respiration and hippocampal peaks (Fig. 2*B*): a respiration-related oscillation with a frequency peak at 0.28 Hz (equal to the respiration rate in that subject) and a co-occurring theta peak at 1.4 Hz (similar to the hippocampal peaks recently reported in humans; Jacobs 2014). Within the hippocampus ($n = 30$), theta peaks ranged from 1 to 3 Hz, whereas frequency of peaks related to natural breathing ranged from 0.24 to 0.37 Hz.

Oscillatory activity in the EEG appears to be hierarchically organized such that amplitude of the oscillations at each characteristic frequency band (gamma, theta, etc.) is modulated by the oscillatory phase of a lower frequency oscillation (Lakatos et al. 2005). This implies that the low-frequency oscillatory activity related to breathing can drive a broadband range of oscillatory activity in the iEEG. The influence of breathing on neuronal activity is not only spatially distributed across the brain but also is in a position to drive a broad frequency range of oscillatory phenomena, as recently suggested by a graph theoretic modeling study (Heck DH, McAfee SS, Liu Y, Babajani-Feremi A, Rezaie R, Freeman WJ, Wheless JW, Papanicolaou AC, Ruszinko M, Kozma R, unpublished observations).

Voluntary pacing of breath. It is known that the automatic vegetative control of breathing can be superseded by higher cognitive factors (Loucks et al. 2007; McKay et al. 2002). Such voluntary pacing of breathing is often employed in cognitive behavioral therapy and meditative/yoga techniques. When our subjects were asked to breathe faster, respiration-locked oscillations were greater in power and continued to follow the breathing frequency at the higher rate, particularly in premotor, caudal-medial frontal, orbitofrontal, and motor cortex, insula, superior temporal gyrus, and amygdala (Fig. 8). As subjects returned to natural breathing, respiration-locked oscillations gradually decreased in power and continued to track at a lower frequency. Previous work (Ito et al. 2014) showed a similar "tracking" effect, with oscillations in the mouse somatosensory cortex when breathing rate was manipulated by producing hypoxic conditions. Although we found respiration-locked oscillations in the somatosensory (parietal) cortex (Fig. 4), we did not observe different coherence between active and passive breathing. The somatosensory cortex involvement is supported by scalp-EEG studies where occlusion of the airways during natural breathing yields an evoked potential over this cortical area (Chan et al. 2015; Davenport et al. 1986). Whereas diaphragm contraction can be seen following stimulation at the vertex of the motor cortex in humans (Gandevia and Rothwell 1987; Foerster 1936), we observed effects throughout the precentral gyrus, including areas corresponding to the face and extremities.

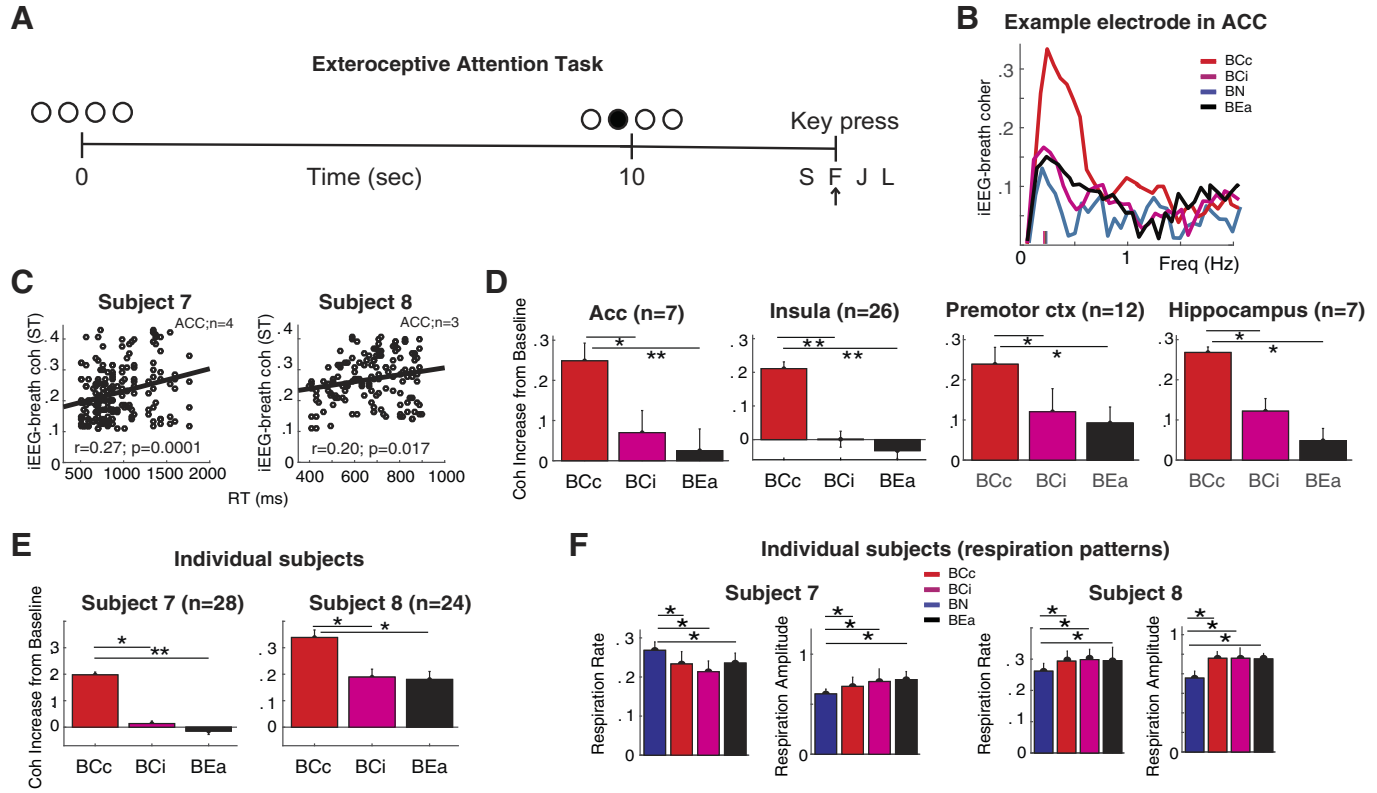

Fig. 10. Increased iEEG-breath coherence through attention is distinct from arousal. *A*: exteroceptive attention task. Subjects pressed the appropriate key to signal a luminance change. *B*: example electrode in the Acc: iEEG-breath coherence increases with effective interoceptive attention to the breath (breath count correct, BCc; red) but remains near natural breathing baseline (breath natural, BN; blue) when attention to the breath is not effective (breath count incorrect, BCi; magenta) or when attention is exteroceptively directed (breath exteroceptive attention, BEa; black). Small vertical lines in *x*-axis indicate respiratory rate. *C*: correlation between iEEG-breath coherence and reaction time in Acc for each subject: trials with slow reaction times showed larger iEEG-breath coherence. *D*: population (2 subjects) iEEG-breath coherence values for the different breathing conditions and brain areas. Values were normalized by the coherence during natural breathing for each electrode site. In all 4 areas examined, BCc was significantly higher than BCi and BEa. *E*: individual subjects' iEEG-breath coherence values for the different breathing conditions averaged across brain areas. *F*: respiration rate and amplitude in the same 2 subjects.

Respiration-locked oscillations were also found in the amygdala, in line with previous human research (Frysinger and Harper 1989a, 1990b). Respiratory patterns are affected by fear/anxiety in humans, indicating involvement of higher cortical and limbic centers (Boiten 1998; Masaoka and Homma 1997; Masaoka et al. 2012). We found stronger respiration-locked oscillations in the amygdala during voluntarily faster breathing compared with natural breathing (Fig. 8). Fast breathing often accompanies high-anxiety states, and it is possible that voluntarily increasing the breathing rate can trigger mechanism similar to those triggered by anxiety (Homma and Masaoka 2008; Masaoka and Homma 1997). Behavioral performance was recently shown to depend on the breathing cycle by Zelano et al. (2016). They showed fear recognition was faster when the stimuli appeared around the inhalation peak, suggesting that oscillatory synchrony in the amygdala depends on the respiratory phase. Our study elaborates on this finding by demonstrating respiration-locked oscillations that follow an experimentally manipulated rate of breathing.

Both amygdala and insula receive projections from the nucleus tractus solitarii (NTS) and medullary cardiorespiratory centers (Gaytán and Pásaro 1998), providing an anatomic pathway potentially subserving this link. We found strong respiration-locked oscillations in the insula, particularly during volitional breathing. The insula is involved in autonomic regulation and interoception (Craig 2003a, 2009b), and neuroimaging studies show posterior insular activation during volitional breathing in humans (Evans et al. 1999; McKay et al. 2002) and rodents (Aleksandrov et al. 2000). Our results also show volitional breathing to result in stronger respiration-locked oscillations in the premotor and olfactory cortices, in line with neuroimaging studies (Evans et al. 1999; Loucks et al. 2007) and in the caudal-medial frontal cortex, an area important for executive control (Evans et al. 1999; Šmejkal et al. 2000) and breathing during exercise (Forster et al. 2012). Volitional breathing also resulted in stronger respiration-locked oscillations in the temporal cortex. Although this may represent breathing-related oscillations driven in sensory cortices, we cannot distinguish this mechanism from the sensory effect of the louder sound emitted during faster breathing, which may entrain the auditory cortex (Schroeder et al. 2014).

Attention to breathing. Distinct from volitional breathing, one can concentrate on the breath itself, a technique used in cognitive behavior therapy and meditation practices (Farb et al. 2013; Levinson et al. 2014). Involvement of frontal lobe areas during breath tracking is suggested by scalp-EEG studies (Giannakodimos et al. 1995; Milz et al. 2014). At a more mechanistic level, we demonstrate increased iEEG-breath coherence in the anterior cingulate cortex (Acc) and premotor cortex (Figs. 9 and 10) when subjects appeared to be more aware of their breath, consistent with the role of these struc-

tures in processing moment-to-moment awareness (Farb et al. 2013; Tang et al. 2010). Notably, the Acc did not show a high degree of respiration-locked oscillations at rest (see Figs. 4 and 5*E*). However, this iEEG-breath coherence changed markedly during breath-awareness (Fig. 9, *B* and *C*). We also found that brain areas involved in interoception, such as the insula (Craig 2003a, 2009b), had stronger respiration-locked oscillations when subjects correctly tracked their breath. The finding of increased hippocampal coherence during breath tracking is consistent with that structure's involvement in the task, which required remembering a count (Sveljo et al. 2010).

The observed stronger iEEG-breath coherence when subjects correctly tracked their breath, compared with when they did not, cannot be explained simply by changes in arousal state. First, alpha power, a proxy of arousal (Cantero et al. 1999; Klimesch et al. 1998), did not differ between correct and incorrect breath-count blocks (Fig. 9*A*, *inset*). Second, respiration rate changes did not impact the effect of attention on iEEG-breath coherence (Fig. 10*F*): both subjects showed increases in coherence despite having different respiratory strategies (*subject 7* showed reduced rate with attention to breath, whereas that for *subject 8* increased). Third, when subjects participated in a task requiring sustained attention to an external stimulus (with arousal levels approximately similar to those during breath tracking; Fig. 10*A*), iEEG-breath coherence did not increase from that observed during natural breathing (Fig. 10, *B–E*). If anything, iEEG-breath coherence in the Acc was weakly reduced as arousal increased (*subject 7*: $r = 0.27$, $P = 0.0001$; *subject 8*, $r = 0.2$, $P = 0.017$).

In other areas, no significant effects of arousal during the exteroceptive attention task were noted. Indeed, iEEG-breath coherence in the Acc during tasks requiring exteroceptive attention may impair performance: because strong iEEG-breath coherence results in increased slow oscillatory power (particularly at the respiratory frequency, Fig. 2*B*), it is tempting to speculate that it may be incompatible with concurrent increases in faster oscillatory rhythms that often support efficient performance in exteroceptive attention tasks (Başar et al. 2001). Conversely, when attention is focused interoceptively, on the breath, as in some meditative practices (e.g., Breath Theravada), high iEEG-breath coherence could be an important neural phenomenon supporting effective breathing concentration.

Respiration rates differed across participants during correct breath counting (Fig. 10*F*; *subject 7* showed slower respiration rate, whereas *subject 8* showed a faster rate). Importantly, both subjects show increased iEEG-breath coherence. A similar effect may occur in the volition rate experiment, suggesting that the increased coherence observed during faster breathing may be explained by the volitional aspects of respiration and not the respiration rate. Future studies using volitional pacing of breathing might explore a pacing that is slower than the spontaneous breathing rate. This would allow us to disambiguate whether the increased coherence observed in our volitional pacing experiment was due to the rate of breathing or the volitional aspects of it. In addition, important statistical efforts have been applied to CFC and coherence computations (e.g., projected CFC/coherence in the complex plane; Miller et al. 2012), rather than the long-time resampling used in the present study), and future studies should take this approach into account.

In summary, our data support the link between respiration and brain activity, proposing respiration rhythms as an organizing principle of cortical oscillations in the human brain, as recently proposed in mice (Tort AB, Ponsel S, Jessberger J, Yanovsky Y, Brankačk J, Draguhn A, unpublished observations). Moreover, respiration rate in humans can be controlled volitionally or attended to while brain activity is measured. In implementing these conditions with concurrent monitoring of breath and intracranial EEG, we demonstrate a network of areas involved in volitional (caudal-medial frontal, premotor, orbitofrontal, and motor cortex, insula, superior temporal gyrus, and amygdala) and attentive breathing (anterior cingulum, premotor, insula, hippocampus), providing insight into potential brain mechanisms involved in therapeutic breathing exercises (Farb et al. 2013; Kemmer et al. 2015; Levinson et al. 2014).

ACKNOWLEDGMENTS

We thank Dr. Nima Mesgarani for intellectual and technical support. We thank Dr. Sean Hwang and Dr. Pierre Megevand for helpful advice on the development of this manuscript and Tucker-Davis Technologies particularly Mark Hanus for technical support.

GRANTS

J. L. Herrero, E. Yeagle, and A. D. Mehta are supported by National Institutes of Health (NIH) Grants U01NS098976-01, R01MH111439, and 1R21MH114166-01. In addition, the work of J. L. Herrero was supported the Human Frontier Science Program Organization (NIH Grant 1R21MH114166-01). S. Khuvis is supported by the Medical Scientist Training Program at the Feinstein Institute for Medical Research and the Hofstra Northwell School of Medicine.

DISCLOSURES

No conflicts of interest, financial or otherwise, are declared by the authors.

AUTHOR CONTRIBUTIONS

J.L.H. conceived and designed research; J.L.H. performed experiments; J.L.H. analyzed data; J.L.H., S.K., E.Y., and A.D.M. interpreted results of experiments; J.L.H. prepared figures; J.L.H. drafted manuscript; J.L.H., S.K., E.Y., M.C., and A.D.M. edited and revised manuscript; J.L.H., S.K., E.Y., M.C., and A.D.M. approved final version of manuscript.

REFERENCES

Aleksandrov VG, Aleksandrova NP, Bagaev VA. Identification of a respiratory related area in the rat insular cortex. *Can J Physiol Pharmacol* 78: 582–586, 2000. doi:10.1139/y00-031.

Başar E, Başar-Eroglu C, Karakaş S, Schürmann M. Gamma, alpha, delta, and theta oscillations govern cognitive processes. *Int J Psychophysiol* 39: 241–248, 2001. doi:10.1016/S0167-8760(00)00145-8.

Biskamp J, Bartos M, Sauer JF. Organization of prefrontal network activity by respiration-related oscillations. *Sci Rep* 7: 45508, 2017. doi:10.1038/srep45508.

Boiten FA. The effects of emotional behaviour on components of the respiratory cycle. *Biol Psychol* 49: 29–51, 1998. doi:10.1016/S0301-0511(98)00025-8.

Borchers S, Hauser TK, Himmelbach M. Bilateral hand representations in human primary proprioceptive areas. *Neuropsychologia* 49: 3383–3391, 2011. doi:10.1016/j.neuropsychologia.2011.08.013.

Brenner RP, Schaul N. Periodic EEG patterns: classification, clinical correlation, and pathophysiology. *J Clin Neurophysiol* 7: 249–267, 1990. doi:10.1097/00004691-199004000-00007.

Bruce EN, Ackerson LM. High-frequency oscillations in human electromyograms during voluntary contractions. *J Neurophysiol* 56: 542–553, 1986.

Butler JE. Drive to the human respiratory muscles. *Respir Physiol Neurobiol* 159: 115–126, 2007. doi:10.1016/j.resp.2007.06.006.

Cantero JL, Atienza M, Salas RM, Gómez CM. Brain spatial microstates of human spontaneous alpha activity in relaxed wakefulness, drowsiness period, and REM sleep. *Brain Topogr* 11: 257–263, 1999. doi:10.1023/A:1022213302688.

Cardoso ER, Rowan JO, Galbraith S. Analysis of the cerebrospinal fluid pulse wave in intracranial pressure. *J Neurosurg* 59: 817–821, 1983. doi:10.3171/jns.1983.59.5.0817.

Chan PY, Cheng CH, Hsu SC, Liu CY, Davenport PW, von Leupoldt A. Respiratory sensory gating measured by respiratory-related evoked potentials in generalized anxiety disorder. *Front Psychol* 6: 957, 2015. doi:10.3389/fpsyg.2015.00957.

Craig AD. Interoception: the sense of the physiological condition of the body. *Curr Opin Neurobiol* 13: 500–505, 2003a. doi:10.1016/S0959-4388(03)00090-4.

Craig AD. How do you feel—now? The anterior insula and human awareness. *Nat Rev Neurosci* 10: 59–70, 2009b. doi:10.1038/nrn2555.

Dale AM, Fischl B, Sereno MI. Cortical surface-based analysis. I. Segmentation and surface reconstruction. *Neuroimage* 9: 179–194, 1999. doi:10.1006/nimg.1998.0395.

Davenport PW, Friedman WA, Thompson FJ, Franzén O. Respiratory-related cortical potentials evoked by inspiratory occlusion in humans. *J Appl Physiol (1985)* 60: 1843–1848, 1986.

Dykstra AR, Chan AM, Quinn BT, Zepeda R, Keller CJ, Cormier J, Madsen JR, Eskandar EN, Cash SS. Individualized localization and cortical surface-based registration of intracranial electrodes. *Neuroimage* 59: 3563–3570, 2012. doi:10.1016/j.neuroimage.2011.11.046.

Evans KC, Shea SA, Saykin AJ. Functional MRI localisation of central nervous system regions associated with volitional inspiration in humans. *J Physiol* 520: 383–392, 1999. doi:10.1111/j.1469-7793.1999.00383.x.

Farb NAS, Segal ZV, Anderson AK. Mindfulness meditation training alters cortical representations of interoceptive attention. *Soc Cogn Affect Neurosci* 8: 15–26, 2013. doi:10.1093/scan/nss066.

Feldman JL, Del Negro CA, Gray PA. Understanding the rhythm of breathing: so near, yet so far. *Annu Rev Physiol* 75: 423–452, 2013. doi:10.1146/annurev-physiol-040510-130049.

Fischl B, Sereno MI, Dale AM. Cortical surface-based analysis. II: Inflation, flattening, and a surface-based coordinate system. *Neuroimage* 9: 195–207, 1999. 10.1006/nimg.1998.0396.

Fischl B, van der Kouwe A, Destrieux C, Halgren E, Ségonne F, Salat DH, Busa E, Seidman LJ, Goldstein J, Kennedy D, Caviness V, Makris N, Rosen B, Dale AM. Automatically parcellating the human cerebral cortex. *Cereb Cortex* 14: 11–22, 2004. doi:10.1093/cercor/bhg087.

Foerster O. Motorische Felder und Bahnen. In: *Handbuch der Neurologie*, edited by Bumke O and Foerster O. Berlin: Springer, 1936, vol. 6, p. 1–357.

Fontanini A, Spano P, Bower JM. Ketamine-xylazine-induced slow (<1.5 Hz) oscillations in the rat piriform (olfactory) cortex are functionally correlated with respiration. *J Neurosci* 23: 7993–8001, 2003.

Forster HV, Haouzi P, Dempsey JA. Control of breathing during exercise. *Compr Physiol* 2: 743–777, 2012. doi:10.1002/cphy.c100045.

Frysinger RC, Harper RM. Cardiac and respiratory correlations with unit discharge in human amygdala and hippocampus. *Electroencephalogr Clin Neurophysiol* 72: 463–470, 1989. doi:10.1016/0013-4694(89)90222-8.

Frysinger RC, Harper RM. Cardiac and respiratory correlations with unit discharge in epileptic human temporal lobe. *Epilepsia* 31: 162–171, 1990. doi:10.1111/j.1528-1167.1990.tb06301.x.

Fumoto M, Sato-Suzuki I, Seki Y, Mohri Y, Arita H. Appearance of high-frequency alpha band with disappearance of low-frequency alpha band in EEG is produced during voluntary abdominal breathing in an eyes-closed condition. *Neurosci Res* 50: 307–317, 2004. doi:10.1016/j.neures.2004.08.005.

Gandevia SC, Rothwell JC. Activation of the human diaphragm from the motor cortex. *J Physiol* 384: 109–118, 1987. doi:10.1113/jphysiol.1987.sp016445.

Gaytán SP, Pásaro R. Connections of the rostral ventral respiratory neuronal cell group: an anterograde and retrograde tracing study in the rat. *Brain Res Bull* 47: 625–642, 1998. doi:10.1016/S0361-9230(98)00125-7.

Gershon RC, Wagster MV, Hendrie HC, Fox NA, Cook KF, Nowinski CJ. NIH toolbox for assessment of neurological and behavioral function. *Neurology* 80, *Suppl* 3: S2–S6, 2013. doi:10.1212/WNL.0b013e3182872e5f.

Giannakodimos S, Ferrie CD, Panayiotopoulos CP. Qualitative and quantitative abnormalities of breath counting during brief generalized 3 Hz spike and slow wave 'subclinical' discharges. *Clin Electroencephalogr* 26: 200–203, 1995. doi:10.1177/155005949502600405.

Greicius MD, Krasnow B, Reiss AL, Menon V. Functional connectivity in the resting brain: a network analysis of the default mode hypothesis. *Proc Natl Acad Sci USA* 100: 253–258, 2003. doi:10.1073/pnas.0135058100.

Groppe DM, Bickel S, Dykstra AR, Wang X, Mégevand P, Mercier MR, Lado FA, Mehta AD, Honey CJ. iELVis: An open source MATLAB toolbox for localizing and visualizing human intracranial electrode data. *J Neurosci Methods* 281: 40–48, 2017. doi:10.1016/j.jneumeth.2017.01.022.

Hamberger MJ, Williams AC, Schevon CA. Extraoperative neurostimulation mapping: results from an international survey of epilepsy surgery programs. *Epilepsia* 55: 933–939, 2014. doi:10.1111/epi.12644.

Harper RM, Poe GR, Rector DM, Kristensen MP. Relationships between hippocampal activity and breathing patterns. *Neurosci Biobehav Rev* 22: 233–236, 1998. doi:10.1016/S0149-7634(97)00010-9.

Heck DH, McAfee SS, Liu Y, Babajani-Feremi A, Rezaie R, Freeman WJ, Wheless JW, Papanicolaou AC, Ruszinkó M, Sokolov Y, Kozma R. Breathing as a fundamental rhythm of brain function. *Front Neural Circuits* 10: 115, 2017. doi:10.3389/fncir.2016.00115.

Herrero JL, Roberts MJ, Delicato LS, Gieselmann MA, Dayan P, Thiele A. Acetylcholine contributes through muscarinic receptors to attentional modulation in V1. *Nature* 454: 1110–1114, 2008. doi:10.1038/nature07141.

Homma I, Masaoka Y. Breathing rhythms and emotions. *Exp Physiol* 93: 1011–1021, 2008. doi:10.1113/expphysiol.2008.042424.

Ito J, Roy S, Liu Y, Cao Y, Fletcher M, Lu L, Boughter JD, Grün S, Heck DH. Whisker barrel cortex delta oscillations and gamma power in the awake mouse are linked to respiration. *Nat Commun* 5: 3572, 2014. doi:10.1038/ncomms4572.

Jacobs J. Hippocampal theta oscillations are slower in humans than in rodents: implications for models of spatial navigation and memory. *Philos Trans R Soc Lond B Biol Sci* 369: 20130304, 2014. doi:10.1098/rstb.2013.0304.

Jenkinson M, Smith S. A global optimisation method for robust affine registration of brain images. *Med Image Anal* 5: 143–156, 2001.

Jenkinson M, Bannister P, Brady M, Smith S. Improved optimization for the robust and accurate linear registration and motion correction of brain images. *Neuroimage* 17: 825–841, 2002.

Jiang H, Schuele S, Rosenow J, Zelano C, Parvizi J, Tao JX, Wu S, Gottfried JA. Theta oscillations rapidly convey odor-specific content in human piriform cortex. *Neuron* 94: 207–219.e4, 2017. doi:10.1016/j.neuron.2017.03.021.

Kaada BR, Jasper H. Respiratory responses to stimulation of temporal pole, insula, and hippocampal and limbic gyri in man. *AMA Arch Neurol Psychiatry* 68: 609–619, 1952. doi:10.1001/archneurpsyc.1952.02320230035004.

Kajikawa Y, Schroeder CE. How local is the local field potential? *Neuron* 72: 847–858, 2011. doi:10.1016/j.neuron.2011.09.029.

Kajimura S, Nomura M. Decreasing propensity to mind-wander with transcranial direct current stimulation. *Neuropsychologia* 75: 533–537, 2015. doi:10.1016/j.neuropsychologia.2015.07.013.

Kemmer PB, Guo Y, Wang Y, Pagnoni G. Network-based characterization of brain functional connectivity in Zen practitioners. *Front Psychol* 6: 603, 2015. doi:10.3389/fpsyg.2015.00603.

Kepecs A, Uchida N, Mainen ZF. Rapid and precise control of sniffing during olfactory discrimination in rats. *J Neurophysiol* 98: 205–213, 2007. doi:10.1152/jn.00071.2007.

Klein A, Ghosh SS, Bao FS, Giard J, Häme Y, Stavsky E, Lee N, Rossa B, Reuter M, Neto EC, Keshavan A. Mindboggling morphometry of human brains. *PLoS Comput Biol* 13: e1005350, 2017. doi:10.1371/journal.pcbi.1005350.

Klimesch W, Doppelmayr M, Russegger H, Pachinger T, Schwaiger J. Induced alpha band power changes in the human EEG and attention. *Neurosci Lett* 244: 73–76, 1998. doi:10.1016/S0304-3940(98)00122-0.

König P, Engel AK, Singer W. Integrator or coincidence detector? The role of the cortical neuron revisited. *Trends Neurosci* 19: 130–137, 1996. doi:10.1016/S0166-2236(96)80019-1.

Krupnik V, Nietzold I, Bartsch B, Rassler B. The effect of motor-respiratory coordination on the precision of tracking movements: influence of attention, task complexity and training. *Eur J Appl Physiol* 115: 2543–2556, 2015. doi:10.1007/s00421-015-3250-5.

Lakatos P, Karmos G, Mehta AD, Ulbert I, Schroeder CE. Entrainment of neuronal oscillations as a mechanism of attentional selection. *Science* 320: 110–113, 2008. doi:10.1126/science.1154735.

Lakatos P, Shah AS, Knuth KH, Ulbert I, Karmos G, Schroeder CE. An oscillatory hierarchy controlling neuronal excitability and stimulus processing in the auditory cortex. *J Neurophysiol* 94: 1904–1911, 2005. doi:10.1152/jn.00263.2005.

Łęski S, Lindén H, Tetzlaff T, Pettersen KH, Einevoll GT. Frequency dependence of signal power and spatial reach of the local field potential. *PLoS Comput Biol* 9: e1003137, 2013. doi:10.1371/journal.pcbi.1003137.

Leth-Steensen C, Elbaz ZK, Douglas VI. Mean response times, variability, and skew in the responding of ADHD children: a response time distributional approach. *Acta Psychol (Amst)* 104: 167–190, 2000. doi:10.1016/S0001-6918(00)00019-6.

Levinson DB, Stoll EL, Kindy SD, Merry HL, Davidson RJ. A mind you can count on: validating breath counting as a behavioral measure of mindfulness. *Front Psychol* 5: 1202, 2014. doi:10.3389/fpsyg.2014.01202.

Locher C, Raux M, Fiamma MN, Morélot-Panzini C, Zelter M, Derenne JP, Similowski T, Straus C. Inspiratory resistances facilitate the diaphragm response to transcranial stimulation in humans. *BMC Physiol* 6: 7, 2006. doi:10.1186/1472-6793-6-7.

Loucks TM, Poletto CJ, Simonyan K, Reynolds CL, Ludlow CL. Human brain activation during phonation and exhalation: common volitional control for two upper airway functions. *Neuroimage* 36: 131–143, 2007. doi:10.1016/j.neuroimage.2007.01.049.

Masaoka Y, Homma I. Anxiety and respiratory patterns: their relationship during mental stress and physical load. *Int J Psychophysiol* 27: 153–159, 1997. doi:10.1016/S0167-8760(97)00052-4.

Masaoka Y, Sugiyama H, Katayama A, Kashiwagi M, Homma I. Remembering the past with slow breathing associated with activity in the parahippocampus and amygdala. *Neurosci Lett* 521: 98–103, 2012. doi:10.1016/j.neulet.2012.05.047.

McKay LC, Evans KC, Frackowiak RS, Corfield DR. Investigation of the neural control of cough and cough suppression in humans using functional brain imaging. *J Appl Physiol (1985)* 95: 1170–1178, 2002. doi:10.1152/japplphysiol.00641.2002.

Mehta AD, Klein G. Clinical utility of functional magnetic resonance imaging for brain mapping in epilepsy surgery. *Epilepsy Res* 89: 126–132, 2010. doi:10.1016/j.eplepsyres.2009.12.001.

Mehta AD, Ulbert I, Schroeder CE. Intermodal selective attention in monkeys. I: distribution and timing of effects across visual areas. *Cereb Cortex* 10: 343–358, 2000. doi:10.1093/cercor/10.4.343.

Miller KJ, Hermes D, Honey CJ, Hebb AO, Ramsey NF, Knight RT, Ojemann JG, Fetz EE. Human motor cortical activity is selectively phase-entrained on underlying rhythms. *PLOS Comput Biol* 8: e1002655, 2012. doi:10.1371/journal.pcbi.1002655.

Miller KJ, Leuthardt EC, Schalk G, Rao RP, Anderson NR, Moran DW, Miller JW, Ojemann JG. Spectral changes in cortical surface potentials during motor movement. *J Neurosci* 27: 2424–2432, 2007a. doi:10.1523/JNEUROSCI.3886-06.2007.

Miller KJ, Schalk G, Fetz EE, den Nijs M, Ojemann JG, Rao RP. Cortical activity during motor execution, motor imagery, and imagery-based online feedback. *Proc Natl Acad Sci USA* 107: 4430–4435, 2010b. doi:10.1073/pnas.0913697107.

Milz P, Faber PL, Lehmann D, Kochi K, Pascual-Marqui RD. sLORETA intracortical lagged coherence during breath counting in meditation-naïve participants. *Front Hum Neurosci* 8: 303, 2014. doi:10.3389/fnhum.2014.00303.

Mitra PP, Pesaran B. Analysis of dynamic brain imaging data. *Biophys J* 76: 691–708, 1999. doi:10.1016/S0006-3495(99)77236-X.

Nguyen Chi V, Müller C, Wolfenstetter T, Yanovsky Y, Draguhn A, Tort AB, Brankačk J. Hippocampal respiration-driven rhythm distinct from theta oscillations in awake mice. *J Neurosci* 36: 162–177, 2016. doi:10.1523/JNEUROSCI.2848-15.2016.

Papademetris X, Jackowski MP, Rajeevan N, DiStasio M, Okuda H, Constable RT, Staib LH. BioImage Suite: an integrated medical image analysis suite: an update. *Insight J* 2006: 209, 2006.

Schroeder CE, Herrero JL, Haegens S. Neuronal dynamics and the mechanistic bases of selective attention. In: *The Oxford Handbook of Attention*, edited by Nobre AC, Kastner S. Oxford: Oxford University Press, 2014, p. 472–508.

Šmejkal V, Druga R, Tintěra J. Brain activation during volitional control of breathing. *Physiol Res* 49: 659–663, 2000.

Sveljo OB, Koprivsek KM, Lucic MA, Prvulovic MB, Culic M. Gender differences in brain areas involved in silent counting by means of fMRI. *Nonlinear Biomed Phys* 4, *Suppl* 1: S2, 2010. doi:10.1186/1753-4631-4-S1-S2.

Tang YY, Lu Q, Geng X, Stein EA, Yang Y, Posner MI. Short-term meditation induces white matter changes in the anterior cingulate. *Proc Natl Acad Sci USA* 107: 15649–15652, 2010. doi:10.1073/pnas.1011043107.

Tenney SM, Ou LC. Ventilatory response of decorticate and decerebrate cats to hypoxia and CO2. *Respir Physiol* 29: 81–92, 1977. doi:10.1016/0034-5687(77)90119-0.

Tort AB, Kramer MA, Thorn C, Gibson DJ, Kubota Y, Graybiel AM, Kopell NJ. Dynamic cross-frequency couplings of local field potential oscillations in rat striatum and hippocampus during performance of a T-maze task. *Proc Natl Acad Sci USA* 105: 20517–20522, 2008. doi:10.1073/pnas.0810524105.

Tsanov M, Chah E, Reilly R, O'Mara SM. Respiratory cycle entrainment of septal neurons mediates the fast coupling of sniffing rate and hippocampal theta rhythm. *Eur J Neurosci* 39: 957–974, 2014. doi:10.1111/ejn.12449.

Urigüen JA, Garcia-Zapirain B. EEG artifact removal-state-of-the-art and guidelines. *J Neural Eng* 12: 031001, 2015. doi:10.1088/1741-2560/12/3/031001.

Vialatte FB, Bakardjian H, Prasad R, Cichocki A. EEG paroxysmal gamma waves during Bhramari Pranayama: a yoga breathing technique. *Conscious Cogn* 18: 977–988, 2009. doi:10.1016/j.concog.2008.01.004.

Welker WI. Analysis of sniffing of the albino rat. *Behaviour* 22: 223–244, 1964. doi:10.1163/156853964X00030.

Zelano C, Jiang H, Zhou G, Arora N, Schuele S, Rosenow J, Gottfried JA. Nasal respiration entrains human limbic oscillations and modulates cognitive function. *J Neurosci* 36: 12448–12467, 2016. doi:10.1523/JNEUROSCI.2586-16.2016.

Zhang H, Fell J, Staresina BP, Weber B, Elger CE, Axmacher N. Gamma power reductions accompany stimulus-specific representations of dynamic events. *Curr Biol* 25: 635–640, 2015. doi:10.1016/j.cub.2015.01.011.